View metadata, citation and similar papers at core.ac.uk
brought to you by CORE
provided by CiteSeerX

Article

JOURNAL OF COMPOSITE MATERIALS

Journal of Composite Materials
2015, Vol. 49(2) 141–162
© The Author(s) 2013
Reprints and permissions:
sagepub.co.uk/journalsPermissions.nav
DOI: 10.1177/0021998313514876
jcm.sagepub.com
SAGE

Dynamic analysis of generally laminated composite beam with a delamination based on a higher-order shear deformable theory

Ramazan-Ali Jafari-Talookolaei[1], Maryam Abedi[2], Mohammad H Kargarnovin[2] and Mohammad T Ahmadian[2]

Abstract

In this study, the dynamic response of the laminated composite beam with arbitrary lay-ups has been investigated within the framework of the third-order shear deformation theory using the finite element method. A new three-nodded finite element compliant with the theory is introduced next. To deal with the dynamic contact between the delaminated segments, unilateral contact constraints are employed in conjunction with Lagrange multiplier method. Furthermore, the Poisson's effect is incorporated in the formulation of the beam constitutive equation. Also, the higher-order inertia effects and material couplings (flexure–tensile, flexure–twist and tensile–twist couplings) are considered in the formulation. Results are extracted based on two methods namely the Eigen-value techniques for frequencies and the Newmark method to calculate the transient response. Then, the obtained results have been verified with the other results available in the literature and very good agreements have been observed. Furthermore, the new results have been obtained for the case where the excitation was due to a moving/non-moving force.

Keywords

Laminated beam, delamination, dynamic analysis, finite element, Lagrange multiplier

Introduction

Structural components made by composite materials are used in many engineering applications. This is due to their superior characters such as high strength-stiffness, lightweight, fatigue resistance etc. Contrary to these mechanical merits, they are subjected to a wide range of defects and damages, which may significantly reduce their structural performance. Among various types of damages that are likely to occur during service in laminated composites, an interlaminar cracking i.e. delamination is the one that mostly to occur.

The angle ply and unsymmetric lay-ups of the composite material have a wide range of applications in different industries. In structures with such type of lay-ups it has been observed that even in a very simple type of structural loading, the flexure, tensile and twist type of deformations are observed, which is essentially due to material couplings causing; flexure–tensile, flexure–twist and tensile–twist couplings. Furthermore, it has been pointed out by numerous researchers that, since the composites have a very low transverse shear modulus compared to their in-plane module, the classical lamination theory (CLT) is not adequate for the analysis of dynamic response even for beam with high slender ratios. Thus, shear deformation is also another important aspect in the analysis of composite structures.

During the past decades, primarily the study of the delaminated composite beams based on the classical theory has received considerable attentions by many researchers. Later on in a few publications the shear

[1]Department of Mechanical Engineering, Islamic Azad University, Sari, Mazandaran Province, Iran
[2]School of Mechanical Engineering, Sharif University of Technology, Tehran, Iran

Corresponding author:
Ramazan-Ali Jafari-Talookolaei, Department of Mechanical Engineering, Islamic Azad University, Sari Branch, P.O. Box 48161-194, Sari, Mazandaran Province, Iran.
Email: ramazanali@gmail.com

Downloaded from jcm.sagepub.com at PENNSYLVANIA STATE UNIV on October 7, 2016

deformation theory are used in which neither of the Poisson's effects and the influences of the material couplings and rotary inertia were considered. The detailed summary of these findings are briefly discussed below.

The free vibrations of an isotropic beam with a through-width delamination by using four Euler–Bernoulli beams connected at the delamination boundaries was studied by Wang et al.[1] The coupling effect of the longitudinal and flexural motions in the delaminated layers was considered in the formulation. It was found that for beams with a short and close to mid-plane delamination the results for the natural frequencies were close to the experimental results. However, according to this study dramatic interpenetration of the delaminated sub-laminates was seen that is physically impossible in the case of off-mid-plane delaminations. This is because the delaminated layers were assumed to deform 'freely' without touching each other (known as *free mode*) and thus have different transverse deformation. To avoid this kind of incompatibility, Mujumdar and Suryanarayan[2] proposed a model based on the assumption that the delaminated layers are constrained to have identical transverse deformations. This was called the *constrained mode* in contrast with the *free mode* proposed by Wang et al. Similar *constrained mode* approach was used by Tracy and Pardoen[3] on a simply supported composite beam analytically and experimentally. Yin and Jane[4] and Chang and Liang[5] have investigated the free and forced vibrations of post-buckled delaminated beams.

Lee et al.[6,7] have performed the free vibration analysis of the composite beam-columns and beams with multiple delaminations. The dynamic characteristics of a delaminated composite beam with two overlapped and non-overlapped delaminations, multiple delaminations and bimaterial beams with single delamination have been studied by Shu and Della[8,9] and Della and Shu.[10–12] Both the '*free mode*' and '*constrained mode*' models have been used in their studies. Recently, the free vibration and time response of the delaminated laminated composite beam (LCB) traversed by the moving force and moving oscillating mass using the Euler–Bernoulli beam theory have been studied by Kargarnovin et al.[13] and Jafari-Talookolaei et al.,[14] respectively.

Valoor and Chandrashekhara[15] extended a model for thick composites beams with symmetric lay-ups to include the effects of the transverse shear deformation and the rotary inertia. In addition, the Poisson's effect was included due to its significance in the analysis of angle-ply laminated beams. They have used the '*constrained mode*' model to represent the free vibrational behavior of the delaminated beam i.e. they have assumed that the sub-laminates in the delamination regions have the identical displacements and rotations. In their analysis, it is assumed that the delamination is at the mid-plane and the in-plane displacement is also ignored.

The '*constrained mode*', however, failed to predict the opening in the mode shapes found in the experiments by Shen and Grady.[16] Luo and Hanagud[17] presented an analytical model based on the Timoshenko beam theory by using linear springs. They have ignored the Poisson's effect in their study. The spring stiffness would then be equal to zero (0) for the *free mode* and infinity (∞) for the *constrained mode*. The effect of coupling between longitudinal and bending vibrations has been considered. This coupling has been noticed by Shen and Grady[16] where it was shown that this coupling has significant effect on the natural frequencies and mode shapes of the delaminated beam. Based on the first-order shear deformation theory (FSDT), Kargarnovin et al.[18] in their work extended the method developed by Valoor and Chandrashekhara[15] and Luo and Hanagud[17] to obtain the dynamic response of the delaminated LCB by considering the Poisson's effect. They have used the *constrained mode* to simulate the motion of the delaminated surfaces. Kargarnovin et al.[19] recently have presented a rather new semi-analytical method towards investigating the free vibration analysis of a delaminated LCB with arbitrary lay-ups. In this work, for the first time the combined effects of material couplings (flexure–tensile, flexure–twist, and tensile–twist couplings) are considered and in addition, the shear deformation, rotary inertia and Poisson's effects are taken into account. The semi-analytical solution for the natural frequencies and mode shapes based on the *free* and *constrained modes* are presented by incorporating the constraint conditions using the method of Lagrange multipliers.

In this paper, the dynamic response of a LCB subjected to the moving/non-moving force has been investigated using a self-developed finite element method by introducing a new higher order beam element. The formulation also accounts the shear deformation, the rotary inertia and material couplings with Poisson's effect included. Eigen-value problems and time responses are analyzed in which the time variables is evaluated by using the Newmark method. In the analysis of time response, the violation of unilateral contact conditions in the delaminated region is prohibited by imposing contact constraints using the Lagrange multipliers. The natural frequencies and time responses obtained from the present study are compared to those of the previously reported results.

Problem modeling

Geometry and material

Consider a thick composite beam of length L and rectangular cross-section of $b \times h$, and containing a

Downloaded from jcm.sagepub.com at PENNSYLVANIA STATE UNIV on October 7, 2016

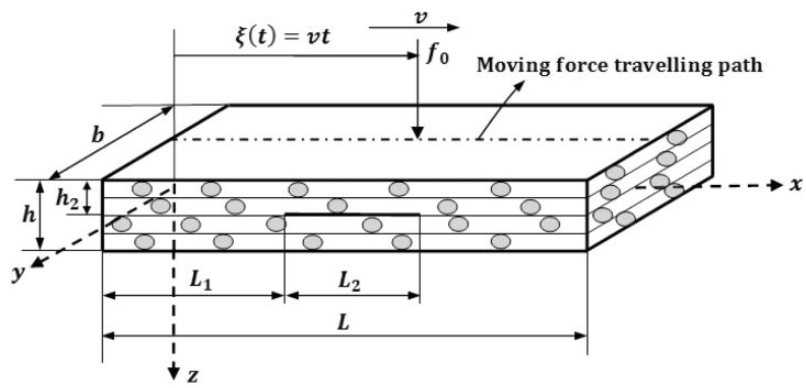

Figure 1. Delaminated composite beam traversed by a moving force.

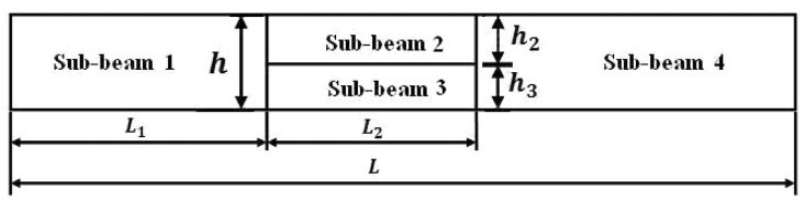

Figure 2. Representation of beam with delamination into four sub-beams.

delamination with length L_2 located at the depth h_2 from the top surface and at a distance L_1 from the left end as shown in Figure 1. It is assumed that the principle axes of each lamina with an arbitrary thickness are oriented at an arbitrary angle θ with respect to the x axis. It should be mentioned that the material of each lamina is considered to be orthotropic. In addition, $\xi(t)$ denotes the location at time t of a constant amplitude moving force of f_0 which enters from the beam left end and moves along the x axis with a constant velocity, v. Hence, the time interval under consideration for the moving force would be $[0, L/v]$. The origin of the global system of coordinate is located at the centroid of the left surface.

As it can be seen from Figure 2, after delamination, the representative beam can be modeled as a combination of four sub-beams connected around the delamination laying between $x = L_1$ up to $x = L_1 + L_2$. In this way, we will have four sub-beams of 1 to 4 with lengths and thicknesses of $L_i \times h_i$ $(i = 1$ to $4)$ where $L_2 = L_3$, $L_4 = L - L_1 - L_2$, $h_1 = h_4 = h$ and h_2 and h_3 the thicknesses of sub-beams 2 and 3, respectively (see Figure 2).

Derivation of kinetic and potential energies for each sub-beam

In this study, we consider an intact LCB made of an orthotropic material. The laminate is made of many unidirectional plies stacked up in different orientation with respect to a reference axis. The length, width, thickness and number of layers of the intact LCB are represented by L, b, h and n, respectively.

The laminated plate constitutive equations based on the third-order shear deformation theory are:[20]

$$\begin{Bmatrix} N_x \\ N_y \\ N_{xy} \\ M_x \\ M_y \\ M_{xy} \\ P_x \\ P_y \\ P_{xy} \end{Bmatrix} = \begin{bmatrix} A_{11} & A_{12} & A_{16} & B_{11} & B_{12} & B_{16} & E_{11} & E_{12} & E_{16} \\ A_{12} & A_{22} & A_{26} & B_{12} & B_{22} & B_{26} & E_{12} & E_{22} & E_{26} \\ A_{16} & A_{26} & A_{66} & B_{16} & B_{26} & B_{66} & E_{16} & E_{26} & E_{66} \\ B_{11} & B_{12} & B_{16} & D_{11} & D_{12} & D_{16} & F_{11} & F_{12} & F_{16} \\ B_{12} & B_{22} & B_{26} & D_{12} & D_{22} & D_{26} & F_{12} & F_{22} & F_{26} \\ B_{16} & B_{26} & B_{66} & D_{16} & D_{26} & D_{66} & F_{16} & F_{26} & F_{66} \\ E_{11} & E_{12} & E_{16} & F_{11} & F_{12} & F_{16} & H_{11} & H_{12} & H_{16} \\ E_{12} & E_{22} & E_{26} & F_{12} & F_{22} & F_{26} & H_{12} & H_{22} & H_{26} \\ E_{16} & E_{26} & E_{66} & F_{16} & F_{26} & F_{66} & H_{16} & H_{26} & H_{66} \end{bmatrix} \begin{Bmatrix} \varepsilon_x^0 \\ \varepsilon_y^0 \\ \varepsilon_{xy}^0 \\ \varepsilon_x^1 \\ \varepsilon_y^1 \\ \varepsilon_{xy}^1 \\ \varepsilon_x^3 \\ \varepsilon_y^3 \\ \varepsilon_{xy}^3 \end{Bmatrix} \quad (1)$$

Downloaded from jcm.sagepub.com at PENNSYLVANIA STATE UNIV on October 7, 2016

In these relations, N_x, N_y and N_{xy} are the in-plane forces, M_x and M_y are the bending and M_{xy} is the twisting moments, P_x and P_y are the higher-order bending moments and P_{xy} is the higher-order twisting moment, $(\varepsilon_x^0, \varepsilon_y^0, \varepsilon_{xy}^0)$ are the mid-plane strains, ε_x^1 and ε_y^1 are the bending and ε_{xy}^1 is the twisting curvatures, ε_x^3 and ε_y^3 are the higher-order bending and ε_{xy}^3 is the higher-order twisting curvatures. Also for the shear forces, we have:

$$\begin{Bmatrix} Q_{yz} \\ Q_{xz} \\ R_{yz} \\ R_{xz} \end{Bmatrix} = \begin{bmatrix} A_{44} & A_{45} & D_{44} & D_{45} \\ A_{45} & A_{55} & D_{45} & D_{55} \\ D_{44} & D_{45} & F_{44} & F_{45} \\ D_{45} & D_{55} & F_{45} & F_{55} \end{bmatrix} \begin{Bmatrix} \gamma_{yz}^0 \\ \gamma_{xz}^0 \\ \gamma_{yz}^2 \\ \gamma_{xz}^2 \end{Bmatrix} \tag{2}$$

where Q_{yz} and Q_{xz} are the resultant shear forces, R_{yz} and R_{xz} are the resultant higher-order shear forces, γ_{yz}^0 and γ_{xz}^0 are the shear strains and γ_{yz}^2 and γ_{xz}^2 are the higher-order shear strains. The coefficients in equations (1) and (2) can be expressed as:[20]

$$(A_{ij}, B_{ij}, D_{ij}, E_{ij}, F_{ij}, H_{ij}) = \sum_{k=1}^{n} \int_{z(k)}^{z(k+1)} \overline{Q}_{ij}^k (1, z, z^2, z^3, z^4, z^6) \mathrm{d}z, \quad (i, j = 1, 2, 6)$$

$$(A_{ij}, D_{ij}, F_{ij}) = \sum_{k=1}^{n} \int_{z(k)}^{z(k+1)} \overline{Q}_{ij}^k (1, z^2, z^4) \mathrm{d}z, \quad (i, j = 4, 5)$$

It should be mentioned that the resultant forces (N, Q and R) and moments (M and P) in equations (1) and (2) are all per unit length.

It should be noted that for the laminated beam, the membrane forces N_y and N_{xy}, the bending moment M_y, the higher-order bending and twisting moments P_y and P_{xy} are all zero.[21] In other words, one can say:

$$\{N_y, N_{xy}, M_y, P_y, P_{xy}\}^T = [b]^T \left\{\varepsilon_x^0, \varepsilon_x^1, \varepsilon_{xy}^1, \varepsilon_x^3\right\}^T + [c]\left\{\varepsilon_y^0, \varepsilon_{xy}^0, \varepsilon_y^1, \varepsilon_y^3, \varepsilon_{xy}^3\right\}^T = \{0\}^T \tag{3}$$

in which:

$$[b] = \begin{bmatrix} A_{12} & A_{16} & B_{12} & E_{12} & E_{16} \\ B_{12} & B_{16} & D_{12} & F_{12} & F_{16} \\ B_{26} & B_{66} & D_{26} & F_{26} & F_{66} \\ E_{12} & E_{16} & F_{12} & H_{12} & H_{16} \end{bmatrix},$$

$$[c] = \begin{bmatrix} A_{22} & A_{26} & B_{22} & E_{22} & E_{26} \\ A_{26} & A_{66} & B_{26} & E_{26} & E_{66} \\ B_{22} & B_{26} & D_{22} & F_{22} & F_{26} \\ E_{22} & E_{26} & F_{22} & H_{22} & H_{26} \\ E_{26} & E_{66} & F_{26} & H_{26} & H_{66} \end{bmatrix}$$

Equation (1) for the remaining resultant force and moments can be rewritten as:

$$\{N_x, M_x, M_{xy}, P_x\}^T = [a]\left\{\varepsilon_x^0, \varepsilon_x^1, \varepsilon_{xy}^1, \varepsilon_x^3\right\}^T + [b]\left\{\varepsilon_y^0, \varepsilon_{xy}^0, \varepsilon_y^1, \varepsilon_y^3, \varepsilon_{xy}^3\right\}^T \tag{4}$$

in which:

$$[a] = \begin{bmatrix} A_{11} & B_{11} & B_{16} & E_{11} \\ B_{11} & D_{11} & D_{16} & F_{11} \\ B_{16} & D_{16} & D_{66} & F_{16} \\ E_{11} & F_{11} & F_{16} & H_{11} \end{bmatrix}$$

Using equation (3), the $(\varepsilon_y^0, \varepsilon_{xy}^0, \varepsilon_y^1, \varepsilon_y^3, \varepsilon_{xy}^3)$ components can be replaced by $(\varepsilon_x^0, \varepsilon_x^1, \varepsilon_{xy}^1, \varepsilon_x^3)$ and by substituting the results in equation (4) one obtains:

$$\begin{Bmatrix} N_x \\ M_x \\ M_{xy} \\ P_x \end{Bmatrix} = \begin{bmatrix} \overline{A}_{11} & \overline{B}_{11} & \overline{B}_{16} & \overline{E}_{11} \\ \overline{B}_{11} & \overline{D}_{11} & \overline{D}_{16} & \overline{F}_{11} \\ \overline{B}_{16} & \overline{D}_{16} & \overline{D}_{66} & \overline{F}_{16} \\ \overline{E}_{11} & \overline{F}_{11} & \overline{F}_{16} & \overline{H}_{11} \end{bmatrix} \begin{Bmatrix} \varepsilon_x^0 \\ \varepsilon_x^1 \\ \varepsilon_{xy}^1 \\ \varepsilon_x^3 \end{Bmatrix} \tag{5}$$

where $(\overline{A}_{11}, \overline{B}_{11}, \text{etc.})$ are the coefficients of the matrix $([a] - [b][c]^{-1}[b]^T)$.

Also, for a laminated beam, the Q_{yz} and R_{yz} are zero. Now, Q_{xz} and R_{xz} can be calculated out of equation (2) as following:

$$\begin{Bmatrix} Q_{xz} \\ R_{xz} \end{Bmatrix} = \begin{bmatrix} \overline{A}_{55} & \overline{D}_{55} \\ \overline{D}_{55} & \overline{F}_{55} \end{bmatrix} \begin{Bmatrix} \gamma_{xz}^0 \\ \gamma_{xz}^2 \end{Bmatrix} = \left(\begin{bmatrix} A_{55} & D_{55} \\ D_{55} & F_{55} \end{bmatrix} - \begin{bmatrix} A_{45} & D_{45} \\ D_{45} & F_{45} \end{bmatrix} \begin{bmatrix} A_{44} & D_{44} \\ D_{44} & F_{44} \end{bmatrix}^{-1} \times \begin{bmatrix} A_{45} & D_{45} \\ D_{45} & F_{45} \end{bmatrix} \right) \begin{Bmatrix} \gamma_{xz}^0 \\ \gamma_{xz}^2 \end{Bmatrix} \tag{6}$$

The strain–displacement relationship can be written as:[20]

$$\varepsilon_x^0 = \frac{\partial u}{\partial x}, \quad \varepsilon_x^1 = \frac{\partial \psi_x}{\partial x}, \quad \varepsilon_{xy}^1 = \frac{\partial \psi_y}{\partial x}, \quad \varepsilon_x^3 = -c_1\left(\frac{\partial \psi_x}{\partial x} + \frac{\partial^2 w}{\partial x^2}\right)$$
$$\gamma_{xz}^0 = \psi_x + \frac{\partial w}{\partial x}, \quad \gamma_{xz}^2 = -3c_1\left(\psi_x + \frac{\partial w}{\partial x}\right) \tag{7}$$

Downloaded from jcm.sagepub.com at PENNSYLVANIA STATE UNIV on October 7, 2016

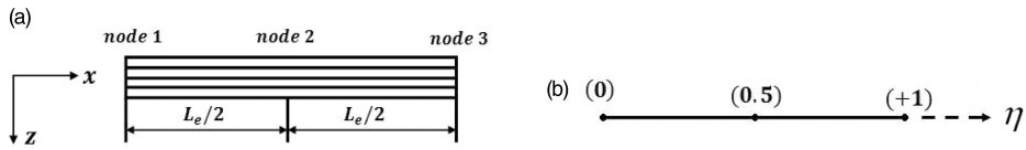

Figure 3. Beam higher-order finite element representation: (a) a three-nodded beam element and (b) its intrinsic coordinates.

in which u and w are the LCB mid-plane displacements in the x and z directions, ψ_x and ψ_y are the mid-plane bending rotations and $c_1 = 4/(3h^2)$.

One of the efficient ways in deriving the governing equations of motion for a system using FEM is to employ the energy principle.[22,23] In implementing this method, one has to derive the stiffness and mass matrices using the kinetic and potential energies of the system.

Now, the potential energy, U, for the LCB can be calculated using the following relationship:[19]

$$U = \frac{1}{2}\int_0^L \Big(N_x\varepsilon_x^0 + M_x\varepsilon_x^1 + M_{xy}\varepsilon_{xy}^1 + P_x\varepsilon_x^3 + Q_{xz}\gamma_{xz}^0 + R_{xz}\gamma_{xz}^2\Big)b\,\mathrm{d}x \tag{8}$$

In the next step, we can express the potential energy in terms of displacement components using equations (5)–(8) as follows:

$$U = \int_0^L \begin{bmatrix} \frac{\overline{A}_{11}}{2}u_{,x}^2 + \frac{\overline{D}_{11} - 2c_1\overline{F}_{11} + c_1^2\overline{H}_{11}}{2}\psi_{x,x}^2 + \frac{\overline{D}_{66}}{2}\psi_{y,x}^2 \\ + \frac{A_{55} - 6c_1D_{55} + 9c_1^2F_{55}}{2}\left(\psi_x^2 + w_{,x}^2\right) + \frac{c_1^2\overline{H}_{11}}{2}w_{,xx}^2 \\ + \left(\overline{B}_{11} - c_1\overline{E}_{11}\right)u_{,x}\psi_{x,x} + \overline{B}_{16}u_{,x}\psi_{y,x} \\ - c_1\overline{E}_{11}u_{,x}w_{,xx} + \left(\overline{D}_{16} - c_1\overline{F}_{16}\right)\psi_{y,x}\psi_{x,x} \\ + \left(c_1^2\overline{H}_{11} - c_1\overline{F}_{11}\right)w_{,xx}\psi_{x,x} - c_1\overline{F}_{16}w_{,xx}\psi_{y,x} \\ + \left(\overline{A}_{55} - 2c_2\overline{D}_{55} + c_2^2\overline{F}_{55}\right)\psi_x w_{,x} \end{bmatrix} b\,\mathrm{d}x \tag{9}$$

Next, we turn to the kinetic energy of the LCB using the following relation:[20]

$$T = \frac{1}{2}\int_0^L \begin{bmatrix} I_1\left(u_{,t}^2 + w_{,t}^2\right) + 2I_2u_{,t}\psi_{x,t} + I_3\left(\psi_{x,t}^2 + \psi_{y,t}^2\right) \\ -2I_4c_1u_{,t}\left(\psi_{x,t} + w_{,xt}\right) \\ -2c_1I_5\left(\psi_{y,t}^2 + \psi_{x,t}^2 + \psi_{x,t}w_{,xt}\right) \\ +I_7c_1^2\left(\psi_{x,t}^2 + \psi_{y,t}^2 + w_{,xt}^2 + 2\psi_{x,t}w_{,xt}\right) \end{bmatrix} b\,\mathrm{d}x \tag{10}$$

in which:

$$(I_1, I_2, I_3, I_4, I_5, I_7) = \int_{-h/2}^{h/2} \rho\left(1, z, z^2, z^3, z^4, z^6\right)\mathrm{d}z$$

It should be mentioned that in all above relations, the symbol ',' used as a subscript stands for the differentiation with respect to any variable followed after it.

Element description

Referred to Figure 3(a), in this study a new higher-order beam element with three nodes, and each node with five degrees of freedom, namely, u_i, w_i, $w_{i,x}$, ψ_{xi} and ψ_{yi} in which u and w are the LCB mid-plane displacements in the x and z directions, respectively, and ψ_x and ψ_y are the mid-plane bending rotations is introduced. The displacements u and w and the rotations ψ_x and ψ_y can thus be interpolated in terms of the intrinsic coordinate (see Figure 3(b)) as:[22]

$$u = \sum_{i=1}^{3} N_i(\eta)u_i, \quad w = \sum_{i=1}^{3}\left(\Lambda_{2i-1}(\eta)w_i + \Lambda_{2i}(\eta)w_{i,x}\right),$$
$$\psi_x = \sum_{i=1}^{3} N_i(\eta)\psi_{xi} \quad \text{and} \quad \psi_y = \sum_{i=1}^{3} N_i(\eta)\psi_{yi} \tag{11}$$

where $N_i(\eta)$ and $\Lambda_j(\eta)$, with $i = 1$–3 and $j = 1$–6, are the Lagrangian and Hermite cubic interpolations, respectively, associated with node i given in Appendix 1. It should be noted that the dimensionless symbol η in equation (11) is:

$$\eta = x/L_e$$

where L_e is the element length of the beam. The vector of element degrees of freedom $\{\delta\}$ is given by:

$$\{\delta\} = \Big\{u_1, w_1, w_{1,x}, \psi_{x1}, \psi_{y1}, u_2, w_2, w_{2,x}, \psi_{x2}, \psi_{y2}, u_3, w_3, w_{3,x}, \psi_{x3}, \psi_{y3}\Big\}^T \tag{12}$$

where superscript T denotes the transpose of a vector or a matrix.

The displacements and rotations of the beam can be related to the nodal degrees of freedom throughout the use of the shape functions to give:

$$u = \lfloor N_u \rfloor\{\delta\} = \lfloor N_1, 0, 0, 0, 0, N_2, 0, 0, 0, 0, N_3, 0, 0, 0, 0\rfloor\{\delta\}$$

Downloaded from jcm.sagepub.com at PENNSYLVANIA STATE UNIV on October 7, 2016

$$
\begin{aligned}
w &= \lfloor N_w \rfloor \{\delta\} \\
&= \lfloor 0, \Lambda_1, \Lambda_2, 0, 0, 0, \Lambda_3, \Lambda_4, 0, 0, 0, \Lambda_5, \Lambda_6, 0, 0 \rfloor \{\delta\} \\
\psi_x &= \lfloor N_{\psi_x} \rfloor \{\delta\} \\
&= \lfloor 0, 0, 0, N_1, 0, 0, 0, 0, N_2, 0, 0, 0, 0, N_3, 0 \rfloor \{\delta\} \\
\psi_y &= \lfloor N_{\psi_y} \rfloor \{\delta\} \\
&= \lfloor 0, 0, 0, 0, N_1, 0, 0, 0, 0, N_2, 0, 0, 0, 0, N_3 \rfloor \{\delta\}
\end{aligned} \tag{13}
$$

Having on hand all primary means, now one can easily calculate the stiffness and mass matrices of the intended LCB which will be dealt with in the next section.

Stiffness and mass matrices of the element

To obtain the stiffness matrix of the beam element, we start by substituting the equation (13) in equation (9) to get the following expression for the stiffness matrix:

$$U = \frac{1}{2}\{\delta\}^T [K^e]\{\delta\} \tag{14}$$

in which the element stiffness matrix is given by:

$$
[K^e] = \int_0^1 \begin{bmatrix}
\overline{A}_{11}\lfloor N_{u,x}\rfloor^T \lfloor N_{u,x}\rfloor + \left(\overline{D}_{11} - 2c_1\overline{F}_{11} + c_1^2\overline{H}_{11}\right)\lfloor N_{\psi_x,x}\rfloor^T \lfloor N_{\psi_x,x}\rfloor + \overline{D}_{66}\lfloor N_{\psi_y,x}\rfloor^T \lfloor N_{\psi_y,x}\rfloor \\
+\left(\overline{A}_{55} - 2c_2\overline{D}_{55} + 9c_1^2\overline{F}_{55}\right)\left(\lfloor N_{\psi_x}\rfloor^T \lfloor N_{\psi_x}\rfloor + \lfloor N_{\psi_x}\rfloor^T \lfloor N_{w,x}\rfloor + \lfloor N_{w,x}\rfloor^T \lfloor N_{w,x}\rfloor + \lfloor N_{w,x}\rfloor^T \lfloor N_{\psi_x}\rfloor\right) \\
+c_1^2\overline{H}_{11}\lfloor N_{w,xx}\rfloor^T \lfloor N_{w,xx}\rfloor + \left(\overline{B}_{11} - c_1\overline{E}_{11}\right)\left(\lfloor N_{u,x}\rfloor^T \lfloor N_{\psi_x,x}\rfloor + \lfloor N_{\psi_x,x}\rfloor^T \lfloor N_{u,x}\rfloor\right) \\
+\overline{B}_{16}\left(\lfloor N_{u,x}\rfloor^T \lfloor N_{\psi_y,x}\rfloor + \lfloor N_{\psi_y,x}\rfloor^T \lfloor N_{u,x}\rfloor\right) - c_1\overline{E}_{11}\left(\lfloor N_{u,x}\rfloor^T \lfloor N_{w,xx}\rfloor + \lfloor N_{w,xx}\rfloor^T \lfloor N_{u,x}\rfloor\right) \\
+\left(\overline{D}_{16} - c_1\overline{F}_{16}\right)\left(\lfloor N_{\psi_y,x}\rfloor^T \lfloor N_{\psi_x,x}\rfloor + \lfloor N_{\psi_x,x}\rfloor^T \lfloor N_{\psi_y,x}\rfloor\right) + \left(c_1^2\overline{H}_{11} - c_1\overline{F}_{11}\right) \\
\times\left(\lfloor N_{w,xx}\rfloor^T \lfloor N_{\psi_x,x}\rfloor + \lfloor N_{\psi_x,x}\rfloor^T \lfloor N_{w,xx}\rfloor\right) - c_1\overline{F}_{16}\left(\lfloor N_{w,xx}\rfloor^T \lfloor N_{\psi_y,x}\rfloor + \lfloor N_{\psi_y,x}\rfloor^T \lfloor N_{w,xx}\rfloor\right)
\end{bmatrix} b\,L_e \mathrm{d}\eta
\tag{15}
$$

On the other hand, substituting from equation (13) into equation (10) and integrating over the element length gives the kinetic energy of the element as:

$$T = \frac{1}{2}\{\delta\}^T [M^e]\{\delta\} \tag{16}$$

where the element mass matrix is:

$$
[M^e] = \int_0^1 \begin{bmatrix}
I_1\left(\lfloor N_u\rfloor^T \lfloor N_u\rfloor + \lfloor N_w\rfloor^T \lfloor N_w\rfloor\right) + (I_2 - c_1 I_4)\left(\lfloor N_u\rfloor^T \lfloor N_{\psi_x}\rfloor + \lfloor N_{\psi_x}\rfloor^T \lfloor N_u\rfloor\right) \\
+\left(I_3 + c_1^2 I_7 - 2c_1 I_5\right)\left(\lfloor N_{\psi_x}\rfloor^T \lfloor N_{\psi_x}\rfloor + \lfloor N_{\psi_y}\rfloor^T \lfloor N_{\psi_y}\rfloor\right) + c_1^2 I_7 \lfloor N_{w,x}\rfloor^T \lfloor N_{w,x}\rfloor \\
+\left(c_1^2 I_7 - c_1 I_5\right)\left(\lfloor N_{w,x}\rfloor^T \lfloor N_{\psi_x}\rfloor + \lfloor N_{\psi_x}\rfloor^T \lfloor N_{w,x}\rfloor\right) - c_1 I_4\left(\lfloor N_u\rfloor^T \lfloor N_{w,x}\rfloor + \lfloor N_{w,x}\rfloor^T \lfloor N_u\rfloor\right)
\end{bmatrix} bL_e \mathrm{d}\eta \tag{17}
$$

The above element stiffness and mass matrices are used to assemble the global corresponding matrices for each sub-beam. It should be mentioned that to obtain the vibrational characteristics of the delaminated LCB based on the *free* and *constrained mode* models, the interacting force between the delaminated sub-beams 2 and 3 can be modeled as a distributed soft spring with stiffness of k (Luo and Hanagud[17]). In this way the total potential energy for the delaminated LCB can be expressed by inclusion of this soft spring in terms of displacements.[22]

Displacement continuity conditions

In order to obtain the stiffness and mass matrices of the whole delaminated LCB, the displacement continuity conditions at the junction between sub-beam 1 with the sub-beams 2 and 3 and also at junction between sub-beam 4 with the sub-beams 2 and 3 has to be enforced. To do this, the overall element nodal displacement vectors and the stiffness and mass matrices of sub-beams 1–4 are considered as $\{\Delta\}_i$, $[K]_i$ and $[M]_i$ ($i = 1$–4), respectively.

Consider now the whole beam's elements at the connecting nodes i, j, k and l for sub-beams 1, 2 and 4 as shown in Figure 4.

Downloaded from jcm.sagepub.com at PENNSYLVANIA STATE UNIV on October 7, 2016

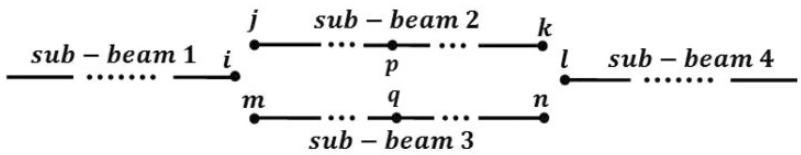

Figure 4. Nodes at the delamination boundaries.

At the connection nodes i–j and k–l, the displacement continuity conditions are as follows:

$$\begin{aligned}
u|_{node\,j} &= \left(u - e_2\psi_x + 4e_2^3/3h^2\left(\psi_x + w_{,x}\right)\right)|_{node\,i},\\
w|_{node\,j} &= w|_{node\,i}, w_{,x}|_{node\,j} = w_{,x}|_{node\,i}, \psi_x|_{node\,j} = \psi_x|_{node\,i},\\
\psi_y|_{node\,j} &= \psi_y|_{node\,i}\\
ut|_{node\,k} &= \left(u - e_2\psi_x + 4e_2^3/3h^2\left(\psi_x + w_{,x}\right)\right)|_{node\,l},\\
w|_{node\,k} &= w|_{node\,l}, w_{,x}|_{node\,k} = w_{,x}|_{node\,l},\\
\psi_x|_{node\,k} &= \psi_x|_{node\,l}, \psi_y|_{node\,k} = \psi_y|_{node\,l}
\end{aligned} \tag{18}$$

where e_2 is the distance between the mid-planes of the sub-beams 1 and 2. In this way, the nodal degrees of freedom for sub-beam 2 i.e. $\{\Delta\}_2$ can be related to the modified nodal degrees of freedom i.e. $\{\underline{\Delta}\}_2$ including the nodal degrees of freedom at nodes i and l plus all of the nodal degrees of freedom for sub-beam 2 except nodes j and k. In other words, one can have:

$$\{\Delta\}_2 = \mathrm{T}_1\{\Delta\}_2 \tag{19}$$

By substituting equation (19) in equations (15) and (17), the following transformation relations for the element stiffness and mass matrices can be established:[22,23]

$$\begin{aligned}
\left[\overline{K}\right]_2 &= [T_1]^T[K]_2[T_1]\\
\left[\overline{M}\right]_2 &= [T_1]^T[M]_2[T_1]
\end{aligned} \tag{20}$$

Assuming the dimension $c_1 \times c_1$ for the stiffness and mass matrices of sub-beam 2 and based on the equation (20), the transformation matrix T_1 has the dimension of $c_1 \times c_1$ and is given as:

$$\begin{cases}
T_1(i,j) = 1 \quad i = j\\
T_1(1,3) = \dfrac{4e_2^3}{3h^2}, \quad T_1(1,4) = \dfrac{4e_2^3}{3h^2} - e_2\\
T_1(c_1-4, c_1-2) = \dfrac{4e_2^3}{3h^2}, \quad T_1(c_1-4, c_1-1) = \dfrac{4e_2^3}{3h^2} - e_2\\
T_1(i,j) = 0, \quad \text{for other}
\end{cases} \tag{21}$$

A similar treatment can be carried out for the connection nodes i–m and n–l and the following transformation relations for the element stiffness and mass matrices can be established:

$$\begin{aligned}
\left[\overline{K}\right]_3 &= [T_2]^T[K]_3[T_2]\\
\left[\overline{M}\right]_3 &= [T_2]^T[M]_3[T_2]
\end{aligned} \tag{22}$$

in which the transformation matrix T_2 has the dimension of the stiffness and mass matrices of sub-beam 3 (i.e. $c_2 \times c_2$) and is given by:

$$\begin{cases}
T_2(i,j) = 1 \quad i = j\\
T_2(1,3) = -\dfrac{4e_3^3}{3h^2}, \quad T_2(1,4) = e_3 - \dfrac{4e_3^3}{3h^2}\\
T_2(c_2-4, c_2-2) = -\dfrac{4e_3^3}{3h^2}, \quad T_2(c_2-4, c_2-1) = e_3 - \dfrac{4e_3^3}{3h^2}\\
T_2(i,j) = 0, \text{ for other}
\end{cases} \tag{23}$$

in which e_3 is the distance between the mid-planes of the sub-beams 1 and 3. The matrices $\left[\overline{K}\right]_i$ and $\left[\overline{M}\right]_i$ $(i = 2, 3)$ will be used to assemble the global stiffness and mass matrices of the whole delaminated LCB.

Dynamic contact condition

As shown in Figure 4, nodes p and q represent two neighboring arbitrary nodes at the upper and lower surfaces of the delaminated segment, respectively. Nodes p and q are called a contact pair. Using the node-to-node model, nodes p and q are in contact if the following condition is satisfied:

$$w_q = w_p \rightarrow w_q - w_p = 0 \tag{24}$$

or in matrix form:

$$\begin{bmatrix} 1 & -1 \end{bmatrix}\begin{Bmatrix} w_q \\ w_p \end{Bmatrix} = \{0\} \tag{25}$$

Depending on the chosen number of elements between nodes j and k, say n elements we will have at most $2n+1$ contact pairs. At any instant of time, we may have not all but limited number of these pairs in contact. For those pairs in contact equation (25) can be established as following:

$$\left[\bar{G}\right]\{\bar{a}\} = \{0\} \tag{26}$$

Downloaded from jcm.sagepub.com at PENNSYLVANIA STATE UNIV on October 7, 2016

where $\left[\bar{G}\right]$ and $\{\bar{a}\}$ are the contact constraint matrix and element nodal vertical displacement of contacted pairs, respectively.

Governing equations of motion

To introduce the constraint equations into the motion governing equations the Lagrange multiplier method is adopted. In general, the finite element equations of motion for the delaminated LCB can be described as:

$$[M]\{\ddot{a}\} + [K]\{a\} + \left[G^T\right]\{\lambda\} = \{F\} = \lfloor N_w \rfloor^T f_0 \quad (27-\text{a})$$

$$[G]\{a\} = \{0\} \quad (27-\text{b})$$

where $[M]$ is global mass matrix, $[K]$ the global stiffness matrix, $[G]$ the global contact constraint matrix for satisfying the non-penetration condition on delaminated segment, $\{\lambda\}$ the Lagrange multiplier vector, $\{F\}$ the external force vector containing the moving force and $\{a\}$ and $\{\ddot{a}\}$ are the global displacement and acceleration vectors of the LCB, respectively. It should be mentioned that $\lfloor N_w \rfloor^T$ is the transpose of the shape functions evaluated at the position of the force. Furthermore, the external force vector is time-dependent that have to be calculated in each time step and not only the contact constraint matrix $[G]$ is a time-depending matrix but geometrically related to the matrix $\left[\bar{G}\right]$. Moreover, $\{a\}$ and $\{\bar{a}\}$ are kinematically related to each other. It should be emphasized that actually λ_i's are the induced contact forces between nodes p and q of two neighboring laminates and when its value is negative, it represents the condition of contact between two contact pairs, and when its value is positive it describes the opening condition between two contact pairs.

Solution method

In order to solve the extracted governing equations, we will divide the solution into two steps. In the first step to get the natural frequencies of *free* and *constrained modes* of delaminated LCB the Eigen-value technique will be employed. The results out of implementing Eigen-value method are compared with those available in the literatures. Then in the next step, the time response of the main problem will be obtained in which the non-penetration condition on delaminated segment will be considered.

The detailed description of the solution methods are presented in following sub-sections.

Eigen-value equations

Based on the procedure outlined in the previous sections, the global equation of motion for the *free* and *constrained modes* of delaminated LCB is:

$$[M]\{\ddot{a}\} + [K]\{a\} = \{0\} \quad (28)$$

Assuming a general solution $\{a\} = \{a_0\}e^{i\omega t}$ for the equation (28), we obtain:

$$\left|[K] - \omega^2[M]\right|\{a_0\} = \{0\} \quad (29)$$

The non-trivial solution for the equation (29) can be obtained by solving equation $\det([K] - \omega^2[M]) = 0$, which yields to the Eigen-values or natural frequencies of the *free* and *constrained modes* of delaminated LCB. Note that $\{a_0\}$ is the corresponding mode shapes to any natural frequencies ω_i.

Time response

To solve the time-dependent equations of motion i.e. equations (27), the Newmark method is employed. The Newmark algorithm is given by:[20]

$$\begin{aligned} \{a\}_{n+1} &= \{a\}_n + \Delta t\{a\} + (0.5-\alpha)\{\ddot{a}\}_n + \alpha\Delta t^2\{\ddot{a}\}_{n+1} \\ \{\dot{a}\}_{n+1} &= \{\dot{a}\}_n + (1-\beta)\Delta t\{\ddot{a}\}_n + \beta\Delta t\{\ddot{a}\}_{n+1} \end{aligned} \quad (30)$$

After substituting equation (30) into equations (27) and doing some mathematics, one can arrive at the following matrix form:

$$\begin{bmatrix} \hat{K} & G_{n+1}^T \\ G_{n+1} & 0 \end{bmatrix} \begin{Bmatrix} a_{n+1} \\ \lambda_{n+1} \end{Bmatrix} = \begin{Bmatrix} \hat{F}_{n+1} \\ 0 \end{Bmatrix} \quad (31)$$

in which:

$$\begin{aligned} \left[\hat{K}\right] &= [K] + \frac{1}{\alpha\Delta t^2}[M], \\ \left\{\hat{F}\right\}_{n+1} &= \{F\}_{n+1} + [M]\frac{1}{\alpha\Delta t^2}(\{a\}_n + \Delta t\{\dot{a}\}_n \\ &\quad + (0.5-\alpha)\Delta t^2\{\ddot{a}\}_n) \end{aligned} \quad (32)$$

where Δt represents time step between t_n and t_{n+1}. The constant coefficients of α and β are the Newmark's parameters which control the integration accuracy and stability of the numerical solution. The values of $\alpha = 0.5$ and $\beta = 0.7$ are picked up in the present study.[24]

The procedure of the dynamic contact algorithm for the iterative method used in the present work is given in Table 1. Based on this algorithm, a MATLAB program is written to calculate the time response of the LCB.

Numerical results and discussion

The validity of the self-developed finite element computer program of the present study breaks into two

Downloaded from jcm.sagepub.com at PENNSYLVANIA STATE UNIV on October 7, 2016

Table 1. The procedure of the dynamic contact algorithm for the iterative method.

A. Initial computations
  A. 1. Form the initial global displacement, velocity and acceleration vectors.
  A.2. Choose the time step Δt and the coefficients α and β of the Newmark method.
  A.3. Form the effective stiffness matrix $\hat{K}$.
B. For every time step
  B.1. Form the effective force vector $\hat{F}$ at current time t_{n+1}.
  B.2. Using the contact constraint matrix at time t_n solve the matrix equations (31) to obtain the displacement vector and Lagrange multipliers vector at current time t_{n+1}.
  B.3. Check each contact pair to satisfy the non-penetration condition and compressive reaction force (i.e. negative value of λ).
    B.3.1. If the relative displacement of each contact pair (i.e. w_q–w_p) is negative; impose the contact constraint on the pair.
    B.3.2. If the reaction force λ is positive; release the node at which the contact constraint is applied.
  B.4. Go to the next time step.

Table 2. Natural frequencies (Hz) of the laminated composite beam (LCB) with a delamination located at the midplane i.e. [0/90/90/0//0/90/90/0].

Mode number	Experiment[25]		Valoor and Chandrashekhara[15]	Zhu et al.[26]	Kargarnovin et al.[18,NR]		Kargarnovin et al.[19]	Present
	Impulse	Sine sweep			WPE	WOPE		
1st	16	17	15.73	15.96	15.78	15.89	15.50	15.61
2nd	98	99	96.86	94.95	97.34	98.05	95.56	96.14
3rd	223	223	224.77	256.74	240.34	242.05	225.92	223.02
4th	441	440	458.32	454.26	414.10	417.28	455.87	443.11

WPE: with Poisson's effects; WOPE: without the Poisson's effects.

parts, part one the validity of Eigen-values and part two validity of the beam's time response.

In the sub-section Calculation of natural frequencies, primarily, for special cases the natural frequencies of the considered problem have been compared with the available results from the literature. Then, for the considered LCB in this study actual natural frequencies under different conditions are obtained. Furthermore, to make sure the developed program is working appropriately, initially the results of time responses for some special cases are compared, then an in-depth time response analysis for the delaminated LCB is presented under the action of non-moving harmonic force and moving constant force (see sub-sections Response to the non-moving harmonic force and Response to the moving constant force).

Calculation of natural frequencies

Example 1. In order to show the accuracy of the presented method for a delaminated LCB, checking on the validity of the results is carried out in this section. In this phase, we preferred to compare our results with those reported in (Okafor et al.,[25] Valoor and Chandrashekhara,[15] Zhu et al.,[26] Kargarnovin et al.[18,19]). The general data in all aforementioned literature are: the beam is 266.7 mm long, 25.4 mm wide and 1.778 mm thick in which the delamination has a length of 101.6 mm with $L_1 = 117.5$ mm. Moreover, the eight-ply laminated beam with lay-up of $[0/90/90/0]_s$ glass/epoxy is considered having material properties taken from Valoor and Chandrashekhara.[15]

In all of the following tables, the double slash '//' signifies the thicknesswise location of the delamination. Also, the WPE and WOPE stand for the case with and without the Poisson's effects, respectively. The fundamental frequencies of the LCB with delamination positioned at the different interfaces one at the time are compared in Tables 2 and 3, for the '*constrained mode*'. It should be mentioned that in all of the following examples, the NR stands for 'Not Reported' and is referred to the results of the authors' previous works (Kargarnovin et al.[18,19]), which are not reported there but are calculated here for the purpose of comparison. Also, it should be noted that if the Poisson's effect is not considered, the results of Kargarnovin et al.[18] should yield to the same results given in Luo and Hanagud.[17]

As it is seen from these tables, good agreement is seen between the calculated results by the present method, the experimental and analytical results of Okafor et al.,[25] Valoor and Chandrashekhara,[15] Zhu et al.,[26] Kargarnovin et al.[18,19] Another important aspect out of results given in these tables is that for the case of cross-ply lay-up, the results of WPE and

Downloaded from jcm.sagepub.com at PENNSYLVANIA STATE UNIV on October 7, 2016

Table 3. Natural frequencies (Hz) of the laminated composite beam (LCB) with a delamination located at different interfaces.

	[0/90/90/0/0//90/90/0]			[0/90/90/0/0/90//90/0]			[0/90/90/0/0/90/90//0]		
	Kargarnovin et al.[18,NR]			Kargarnovin et al.[18,NR]			Kargarnovin et al[18,NR]		
Mode number	WPE	WOPE	Present	WPE	WOPE	Present	WPE	WOPE	Present
1st	15.80	15.91	15.71	15.80	15.91	15.80	15.90	16.01	15.87
2nd	96.54	97.26	97.06	95.88	96.55	97.90	97.64	98.39	98.70
3rd	244.21	246.10	243.11	246.69	248.40	249.52	258.99	260.92	259.51
4th	426.60	429.87	419.22	435.55	438.57	434.22	464.75	468.02	460.44

WPE: with Poisson's effects; WOPE: without the Poisson's effects.

Table 4. Normalized free mode frequencies of symmetric angle-ply $[10^\circ/-10^\circ/10^\circ/-10^\circ]_s$ delaminated beams ($L/h = 15$).

	C-C		C-H		H-H		C-F	
Mode No.	Kargarnovin et al.[19]	Present	Kargarnovin et al.[19]	Present	Kargarnovin et al.[19]	Present	Kargarnovin et al.[19]	Present
1	4.0746	4.2382	2.9365	3.0608	1.7465	1.9765	0.8075	0.8708
2	10.0070	9.8991	9.0788	9.0344	8.0505	8.0551	3.7746	3.8618
3	11.4243^L	11.5712^L	11.3997^L	10.4325^L	11.3903^L	10.8282^L	4.5070^T	4.7430^T
4	12.9340^T	11.9615^T	12.8446^T	12.4802^T	12.8115^T	12.3909^T	10.7286	10.9499
5	15.8929	15.7893	15.2422	15.1889	14.4463	13.7458	11.4672^L	11.2505^L
6	17.3677^T	17.4567^T	17.3504^T	16.7164^T	17.3411^T	17.0697^T	17.7072	15.2041
7	23.1155	22.4646	22.5811	21.7564	22.3717	21.7392	15.2746^T	17.8143^T
8	31.2636	31.0143	30.9555	26.7687	30.6541	30.6451	24.9776	24.7644

^{L}Indicating the longitudinal vibrations; ^{T}Indicating the torsional vibrations.

WOPE are almost the same. This conclusion is mentioned by many authors in the literatures (Krishnaswamy et al.;[27] Jun et al.,[28] Kadivar and Mohebpour[29]).

Example 2. In this example and all subsequent ones the width of the beam is taken as unity and the thickness of all layers in the LCB is equal. Moreover, AS4/3501 Graphite-Epoxy is chosen for the LCB having the following mechanical properties (Krishnaswamy et al.[27]):

$$E_{11} = 144.8\,\text{GPa}, \quad E_{22} = 9.65\,\text{GPa}, \quad G_{12} = 4.14\,\text{GPa},$$
$$G_{13} = 4.14\,\text{GPa}, \quad G_{23} = 3.45\,\text{GPa}, \quad \upsilon_{12} = 0.33,$$
$$\rho = 1389.23\,\text{kg/m}^3$$

Also, the calculated natural frequencies in these examples are presented in a dimensionless form of ($\Omega = \omega/\sqrt{\frac{E_{11}H^2}{\rho L^4}}$) and the following are other non-dimensional parameters used in our analysis:

$$\overline{L}_1 = \frac{L_1}{L}, \quad \overline{L}_2 = \frac{L_2}{L}, \quad \overline{h}_2 = \frac{h_2}{h}$$

Consider an angle-ply LCB with a central delamination located at the mid-plane and symmetric stacking sequence of $[10/-10/10/-10]_s$. The first five fundamental frequencies of such beam based on the *free mode* under various movable boundary conditions are calculated and compared in Table 4. The beam has the slenderness ratio of $L/h = 15$ and the non-dimensional delamination length is $\overline{L}_2 = 0.2$. In this table, C, H and F stand for Clamped, Hinged and Free boundary conditions. Note that in this table for example, for the case of C-C, the third row is referred to the longitudinal mode and forth and sixth rows represent the results for the torsional modes.

Based on presented results in Table 4, it should be highly emphasized that disregarding of any coupling effects for example longitudinal-torsional modes will lead the designers to some wrong conclusions specially when the LCB is vibrating in one of these modes due to coupling effects (see highlighted cells in the table).

Example 3. In order to show the importance of the Poisson's effect for the dynamic analysis of the angle-ply LCB, the normalized fundamental frequency of the C-C and C-H beam comprising of four laminas with

Downloaded from jcm.sagepub.com at PENNSYLVANIA STATE UNIV on October 7, 2016

symmetric lay-up shown in Figure 5 is presented in Tables 5 and 6. The dimensionless length of the single delamination is 0.2 and it will be placed in different interfaces one at a time. It should be mentioned that despite considering laminated beam theory in reference Chandrashekhara et al.[30] no Poisson's effect is considered in there whereas in the reference Krishnaswamy et al.[27] this effect is included.

From the results given in these tables as it is expected, for the unidirectional ($\theta = 0°$) or cross-ply ($\theta = 90°$) LCB the inclusion of Poisson's effect produces no significant changes on the fundamental frequency. Contrary to this, the fundamental frequency for an angle-ply beam with no Poisson's effect deviates significantly from the exact value (i.e. considering Poisson's effect), especially for the layout angle between 30° and 60°.

Example 4. To find the real natural frequencies of the delaminated LCB, the cantilever beam comprising of four laminas with unsymmetric lay-up shown in Figure 6 is considered. The dimensionless length of the delamination is 0.2 or 0.4 or 0.6 or 0.8 one at a time. As can be seen from Tables 7–9, the natural frequencies obtained from the '*free*' mode model represents the lower bound and the '*constrained*' mode model signifies the upper bound of the real solutions. This has been also mentioned in many other studies (Della and Shu,[10–12] Kargarnovin et al.[19]).

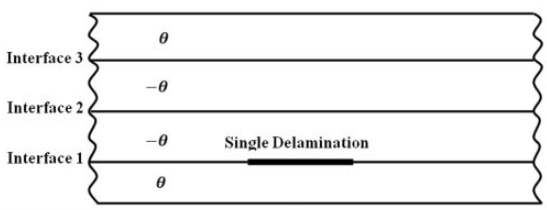

Figure 5. An LCB with $[\theta/-\theta/-\theta/\theta]$ lay-up and a central delamination.

Based on the results given in Tables 7–9, if this single delamination is located at the interfaces 2 or 3, the natural frequencies of the beam under *free* and *constrained modes* become the same as the *physically-real mode* (PRM), which signifies that no 'opening mode' is happening. It should be emphasized that in PRM, which is suggested in this study, the opening is allowed but no penetration can occur; but when the delamination is located at the interface 1, the so-called 'opening modes' may appear more easily even for a short-length delamination. It should be mentioned that though the thicknesswise distance of the interface 1 and 3 is the same from the free surfaces, the opening mode is only seen when the delamination is located at the interface 1. This could be due to the fact that when the delamination is placed at the interface 3. the stiffness values of sub-beams [0°] and [45°/0°/45°] yield almost to the same results. On the other hand, when the delamination is placed at the interface 1, the difference between the stiffness values of the clustered sub-beams 2 with [0°/45°/0°] lay-ups and sub-beam 3 with [45°] lay-up becomes relatively high, which leads to different deformations in two adjacent sub-beams 2 and 3 causing opening mode. This phenomenon can also be

Table 5. Normalized free mode frequencies of angle-ply laminated composite beam (LCB) for C-C boundary conditions ($L/h = 15$).

Thickness-wise location of delamination	θ(°)	0	15	30	45	60	75	90
Interface 1 or 3	Present- WPE	4.5026	3.6139	2.5538	1.8059	1.6095	1.5912	1.5987
	Present- WOPE	4.5287	3.8856	3.1247	2.6610	1.9136	1.6132	1.6178
	WPE[18,NR]	4.9325	4.0254	2.8505	1.9234	1.6312	1.6088	1.6187
	WOPE[18,NR]	4.9411	4.7468	4.1566	3.2129	2.2080	1.6855	1.6233
Interface 2	Present- WPE	4.6457	3.7039	2.5700	1.8345	1.5992	1.5804	1.5866
	Present- WOPE	4.6567	3.9064	3.0951	2.5634	1.9200	1.6082	1.5903
	WPE[18,NR]	4.9628	4.1889	2.9759	1.9531	1.6332	1.6095	1.6194
	WOPE[18,NR]	4.9716	4.7741	4.1754	3.2216	2.2105	1.6863	1.6240
Intact	Present	4.7401	3.7846	2.7243	1.8490	1.5923	1.5872	1.5902
	Krishnaswamy et al.[27]	4.869	3.988	2.878	1.947 (1.8472[a])	1.644	1.621	1.631
	Chandrashekhara et al.[30]	4.849	4.664	4.098	3.184	2.198	1.682	1.620

WPE: with Poisson's effects; WOPE: without the Poisson's effects.
[a]From Chandrashekhara and Bangera[31] Based on the third-order shear deformation theory.

Downloaded from jcm.sagepub.com at PENNSYLVANIA STATE UNIV on October 7, 2016

Table 6. Normalized free mode frequencies of angle-ply laminated composite beam (LCB) for C-H boundary conditions ($L/h = 15$).

Thickness-wise location of delamination	$\theta(^\circ)$	0	15	30	45	60	75	90
Interface 1 or 3	Present- WPE	3.6394	2.7586	1.8305	1.2341	1.0885	1.0759	1.0822
	Present- WOPE	3.6401	3.0241	2.4190	1.7532	1.3764	1.1053	1.0945
	WPE[18,NR]	3.7755	2.9725	2.0311	1.3438	1.1345	1.1190	1.1262
	WOPE[18,NR]	3.7838	3.6049	3.0844	2.3121	1.5513	1.1737	1.1295
Interface 2	Present- WPE	3.2415	2.6132	1.8869	1.2197	1.0782	1.0657	1.0714
	Present- WOPE	3.2418	2.7802	2.3763	1.8041	1.2365	1.0983	1.0942
	WPE[18,NR]	3.7861	3.0939	2.1154	1.3592	1.1314	1.1151	1.1223
	WOPE[18,NR]	3.7945	3.6130	3.0864	2.3089	1.5468	1.1697	1.1256
Intact	Present	3.6872	2.8324	1.9456	1.3075	1.1210	1.0982	1.0921
	Krishnaswamy et al.[27]	3.837	3.243	2.213	1.388	1.146	1.129	1.136
	Chandrashekhara et al.[30]	3.731	3.559	3.057	2.303	1.551	1.175	1.131

WPE: with Poisson's effects; WOPE: without the Poisson's effects.

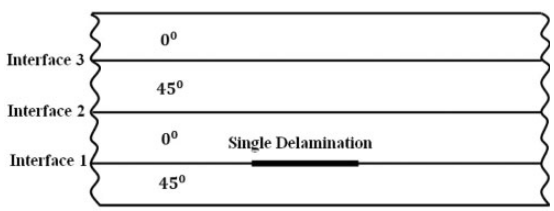

Figure 6. An LCB with [0/45/0/45] lay-ups and a single central delamination.

justified by considering the bending stiffness of sub-beams 2 and 3 presented in Table 10.

Response to the non-moving harmonic force

A delaminated LCB with clamped-free boundary conditions and lay-ups shown in Figure 7 is considered here. The concentrated harmonic force which is applied at the free end (i.e. $x = L$) is changing as:

$$f(x,t) = f_0 \sin(\bar{\omega} t)\delta(x - L)$$

where $f_0 = 0.5$ N and $\overline{\omega}$ could take the values of 10, 30 and 50 rad/s one at a time and ä is the Dirac-Delta function. The central delamination is located at interface 1 and its normalized length could be 0.2 or 0.8 one at a time.

In Figure 7, A and B are two central neighboring points in each sub-beam above and below of delamination and C is another point at center of end section. We are going to study the effect of changing $\bar{\omega}$ and delamination length on the dynamic deflections of these three points.

Note that in evaluating the dynamic response (DR) of the delaminated LCB, two different conditions for the dynamic contacts are considered. That is non-physically real mode (NPRM) which allows penetration and PRM condition which has been defined before. Figures 8 and 9 show the DR variation of points A, B and C in a delaminated LCB under variations of the $\bar{\omega}$ and delamination length. In these figures, the response which excludes the contact is obtained using the *free mode* model. Note that in Figure 8, which illustrates the DR for $\overline{L}_2 = 0.2$, no significant difference is seen between the DR of points A and B. However, at Figure 9, this difference is more notable due to the increase in the length of delamination. Moreover, by comparison of DRs between including and excluding dynamic contact conditions, the opening mode shows itself more clearly as the delamination length increases. In general, this means that the effect of the dynamic contact and delamination length on the dynamic response of the delaminated LCB is found to be significant especially for longer delamination. Also, neglecting the dynamic contact between the delaminated interfaces results in the inter-penetration of the points laying in the interfaces of the delaminated segments.

It should be mentioned that the dynamic response of the delaminated LCB is greatly dependent on the frequency of the exciting force. As expected, the closer the exciting frequency is to the fundamental natural frequency of the delaminated LCB (see Table 7: $\omega_1 = 28$ rad/sec), the greater the response amplitude would be. This phenomenon is obviously seen by the dynamic deflection at point C in Figures 8 and 9.

Response to the moving constant force

In this section, we will analyze the response of the delaminated beam under the action of a constant single moving force. Figures 10–12 show the variation of

Downloaded from jcm.sagepub.com at PENNSYLVANIA STATE UNIV on October 7, 2016

Table 7. Dimensionless fundamental frequencies of the laminated composite beam (LCB) with delamination located at interface 1 ($L/h = 15$).

	Jafari-Talookolaei et al.[14,NR]		Kargarnovin et al.[18,NR]		Kargarnovin et al.[19,NR]		Present		
$\bar{L}_2$	WPE	WOPE	WPE	WOPE	Free	Cons.	Free	Cons.	PRM
0.2	0.7995	0.8194	0.7283	0.7993	0.6815	0.6815	0.6546	0.6547	0.6547
0.4	0.7948	0.8115	0.7232	0.7927	0.6776	0.6790	0.6526	0.6532	0.6530
0.6	0.7829	0.7951	0.7156	0.7790	0.6684	0.6734	0.6346	0.6401	0.6382
0.8	0.7624	0.7688	0.7046	0.7566	0.6102	0.6686	0.5943	0.6348	0.6237

Cons.: constrained mode; WPE: with Poisson's effects; WOPE: without the Poisson's effects.

Table 8. Dimensionless fundamental frequencies of the laminated composite beam (LCB) with delamination located at interface 2 ($L/h = 15$).

	Jafari-Talookolaei et al.[14,NR]		Kargarnovin et al.[18,NR]		Kargarnovin et al.[19,NR]		Present		
$\bar{L}_2$	WPE	WOPE	WPE	WOPE	Free	Cons.	Free	Cons.	PRM
0.2	0.7948	0.8180	0.7285	0.7970	0.6748	0.6748	0.6578	0.6578	0.6578
0.4	0.7603	0.7896	0.7035	0.7697	0.6280	0.6280	0.6009	0.6009	0.6009
0.6	0.6878	0.7274	0.6495	0.7109	0.5403	0.5403	0.5287	0.5287	0.5287
0.8	0.5958	0.6437	0.5765	0.6314	0.4449	0.4449	0.4260	0.4260	0.4260

Cons.: constrained mode; PRM: physically-real mode; WPE: with Poisson's effects; WOPE: without the Poisson's effects.

Table 9. Dimensionless fundamental frequencies of the laminated composite beam (LCB) with delamination located at interface 3 ($L/h = 15$).

	Jafari-Talookolaei et al.[14,NR]		Kargarnovin et al.[18,NR]		Kargarnovin et al.[19,NR]		Present		
$\bar{L}_2$	WPE	WOPE	WPE	WOPE	Free	Cons.	Free	Cons.	PRM
0.2	0.7960	0.8156	0.7188	0.7952	0.6750	0.6750	0.6590	0.6590	0.6590
0.4	0.7685	0.7836	0.6614	0.7656	0.6296	0.6296	0.6036	0.6036	0.6036
0.6	0.7083	0.7174	0.5619	0.7014	0.5440	0.5440	0.5329	0.5329	0.5329
0.8	0.6271	0.6307	0.4582	0.6226	0.4992	0.4992	0.4310	0.4310	0.4310

Cons.: constrained mode; PRM: physically-real mode; WPE: with Poisson's effects; WOPE: without the Poisson's effects.

Table 10. Bending stiffness ($\bar{D}_{11}$ (Pa)) for sub-beams 2 and 3.

Interface 1		Interface 2		Interface 3	
Sub-beam 2	Sub-beam 3	Sub-beam 2	Sub-beam 3	Sub-beam 2	Sub-beam 3
4.92895 (10^9)	1.57028 (10^7)	8.17820 (10^8)	8.17820 (10^8)	1.88542 (10^8)	5.96492 (10^8)

the dynamic magnification factor (DMF) vs. dimensionless time (T_f/τ) and Figures 13–15 illustrate the deflection variation at the beam's center ($\overline{w}_m$) expressed in metric unit at the force critical velocity vs. $\overline{x}_f$ under variations of different parameters. Note that the DMF represents the ratio of the maximum magnitude of the dynamic deflection at the beam's center to the corresponding static values of the intact beam. The symbol T_f denotes the fundamental period of the intact beam and τ represents the traveling time of the moving force from

Downloaded from jcm.sagepub.com at PENNSYLVANIA STATE UNIV on October 7, 2016

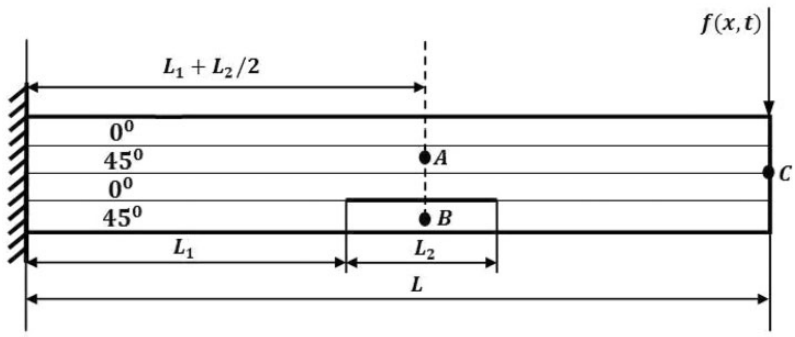

Figure 7. Cantilever delaminated LCB excited by a harmonic force at the free end ($L/h = 15$).

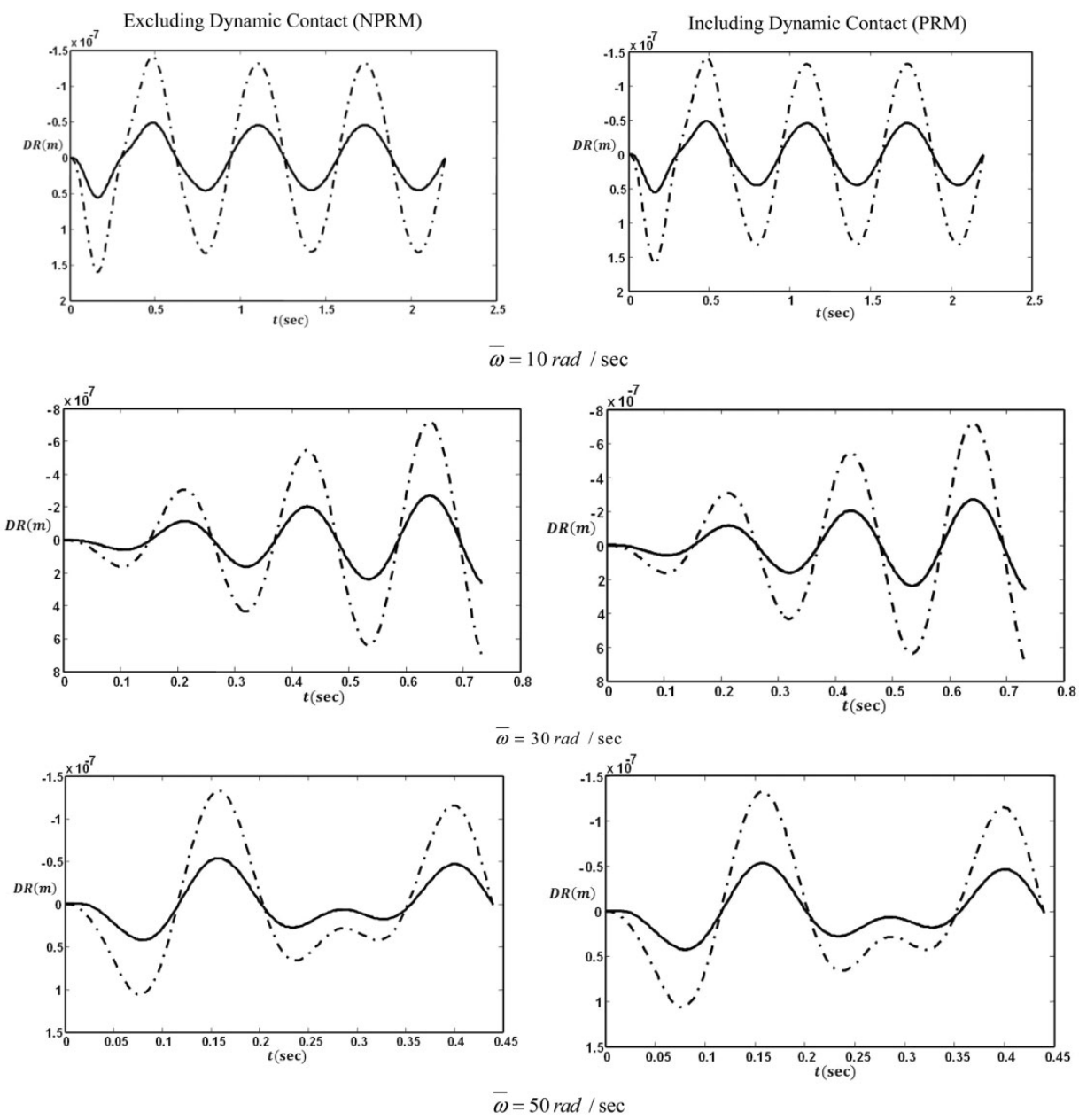

Figure 8. Dynamic response of the delaminated LCB $(\bar{L}_2 = 0.2)$ (Solid Line: Point A, Dashed Line: Point B, Dashed-Dot Line: Point C). NPRM: non-physically real mode; PRM: physically real mode.

Downloaded from jcm.sagepub.com at PENNSYLVANIA STATE UNIV on October 7, 2016

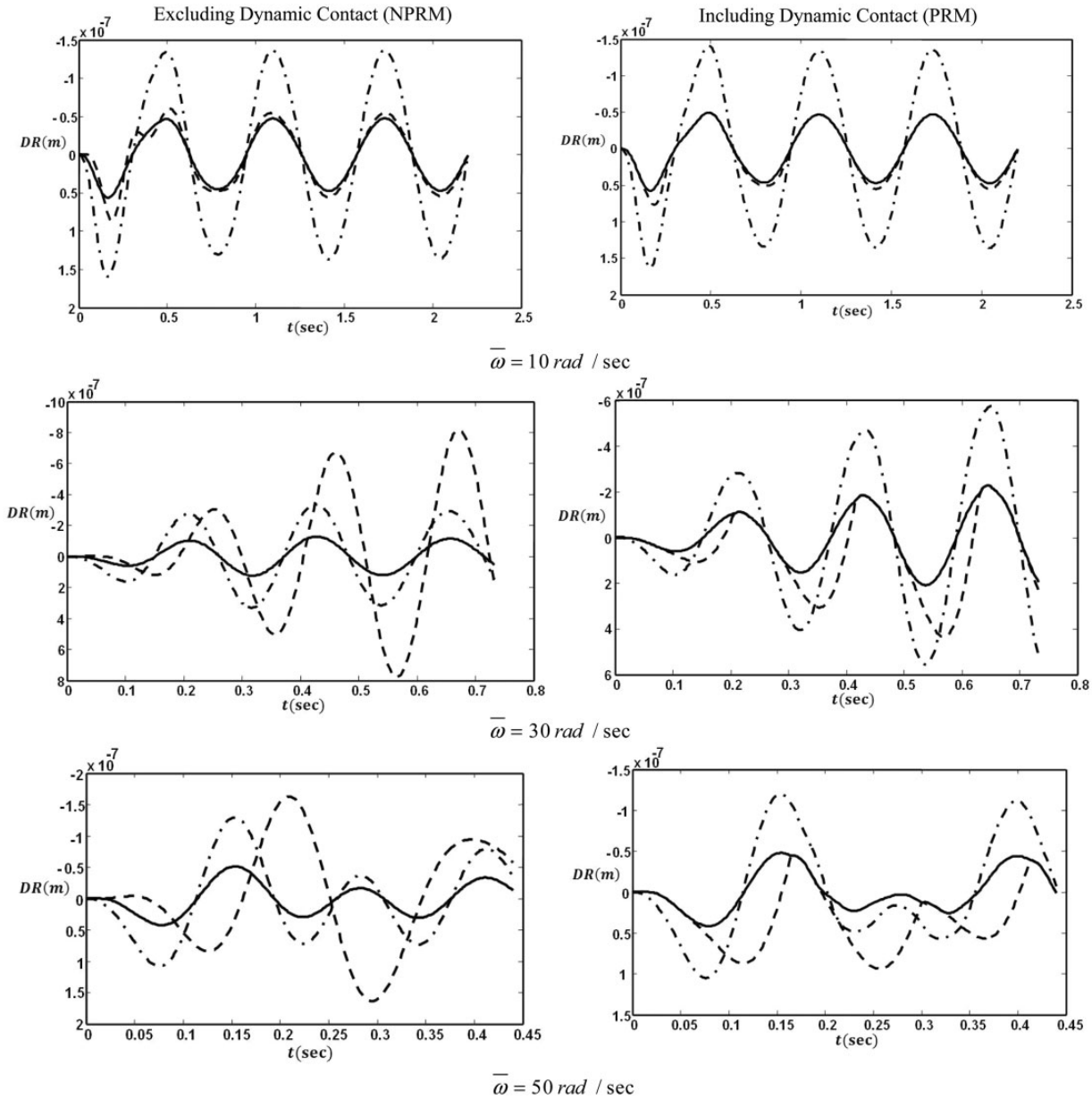

Figure 9. Dynamic response of the delaminated LCB $(\overline{L}_2 = 0.8)$ (Solid Line: Point A, Dashed Line: Point B, Dashed-Dot Line: Point C).
NPRM: non-physically real mode; PRM: physically real mode.

the left end to the right end of the beam ($\tau = L/v$). Moreover, $\overline{x}_f$ is the non-dimensional time (t/τ) equivalent to the non-dimensional horizontal position of moving force (vt/L). In addition, the critical velocity (V_{cr}) is the velocity in which the maximum DMF occurs.

It has to be emphasized that the results presented in Figures 10–15 are all related to a simply supported beam with a moveable end and slenderness ration $L/h = 15$. Nonetheless, similar analysis can be done with no difficulties for other types of boundary conditions. From the static analysis related to the equilibrium condition of a simply supported intact beam, the maximum static deflection due to only the concentrated force f_0 located at the mid-span is $f_0 L^3/(48\,\overline{D}_{11,1})$. In these figures, solid and dashed lines are the DMF for points A and B, respectively, that their geometrical locations are shown in Figure 7. Also, DMF obtained from CLT (Jafari-Talookolaei et al.[14]) and FSDT (Kargarnovin et al.[18]) based on the WPE are shown with dotted and dashed-dotted lines, respectively.

A close inspection of Figures 10–15 reveals that out of three employed methods, the CLT predicts least value for the maximum dynamic response whereas the presented formulation in this paper gives the highest

Downloaded from jcm.sagepub.com at PENNSYLVANIA STATE UNIV on October 7, 2016

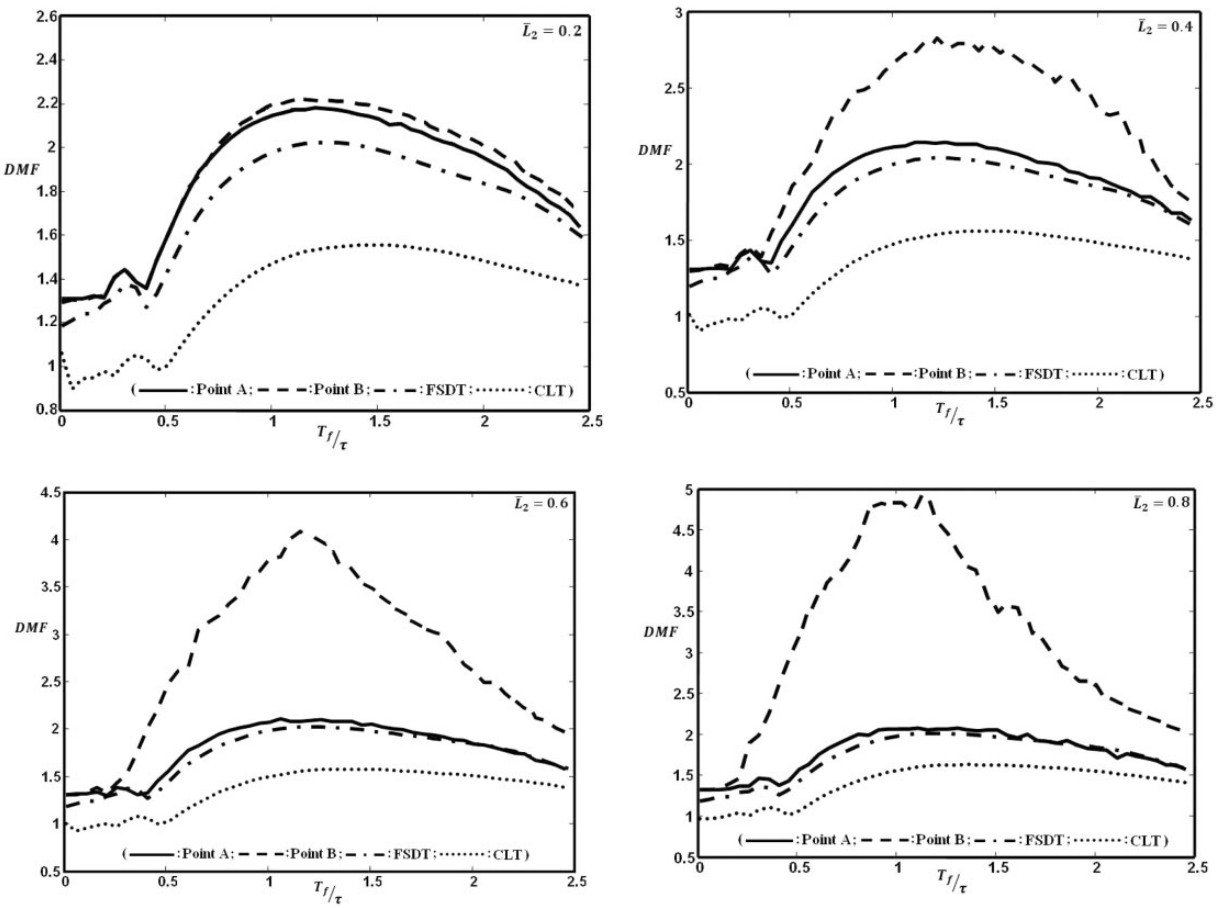

Figure 10. Variation of DMF vs. T_f/τ for different delamination lengths (delamination located at interface 1). DMF: dynamic magnification factor. CLT: classical lamination theory.
CLT: classical lamination theory; FSDT: first-order shear deformation theory.

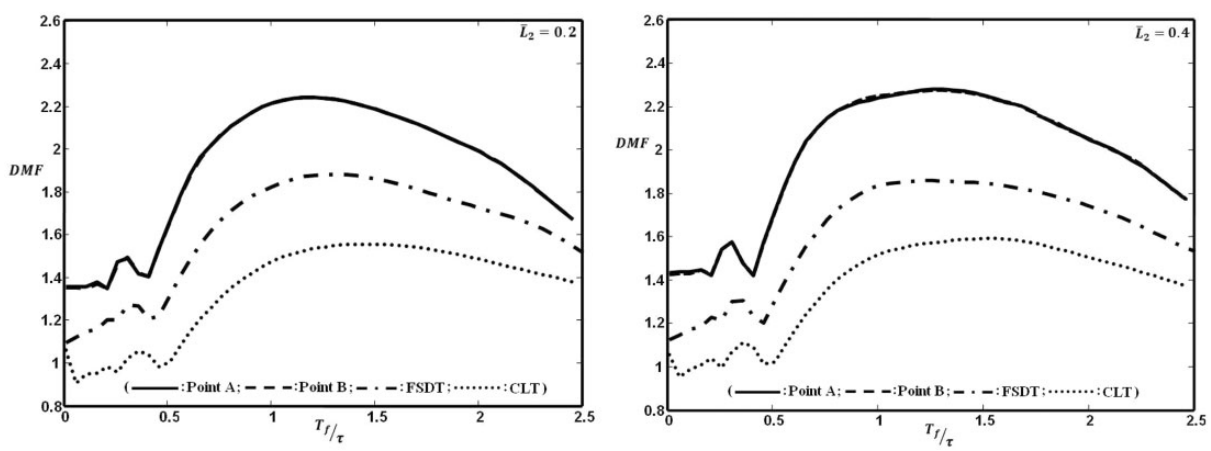

Figure 11. Variation of DMF vs. T_f/τ for different delamination lengths (delamination located at interface 2). DMF: dynamic magnification factor.
CLT: classical lamination theory; FSDT: first-order shear deformation theory.

Downloaded from jcm.sagepub.com at PENNSYLVANIA STATE UNIV on October 7, 2016

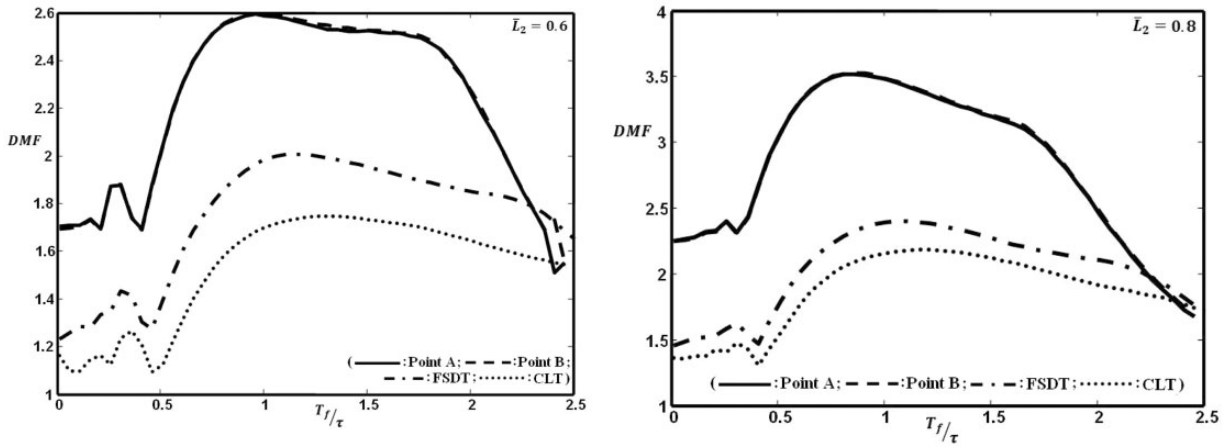

Figure 11. Continued.

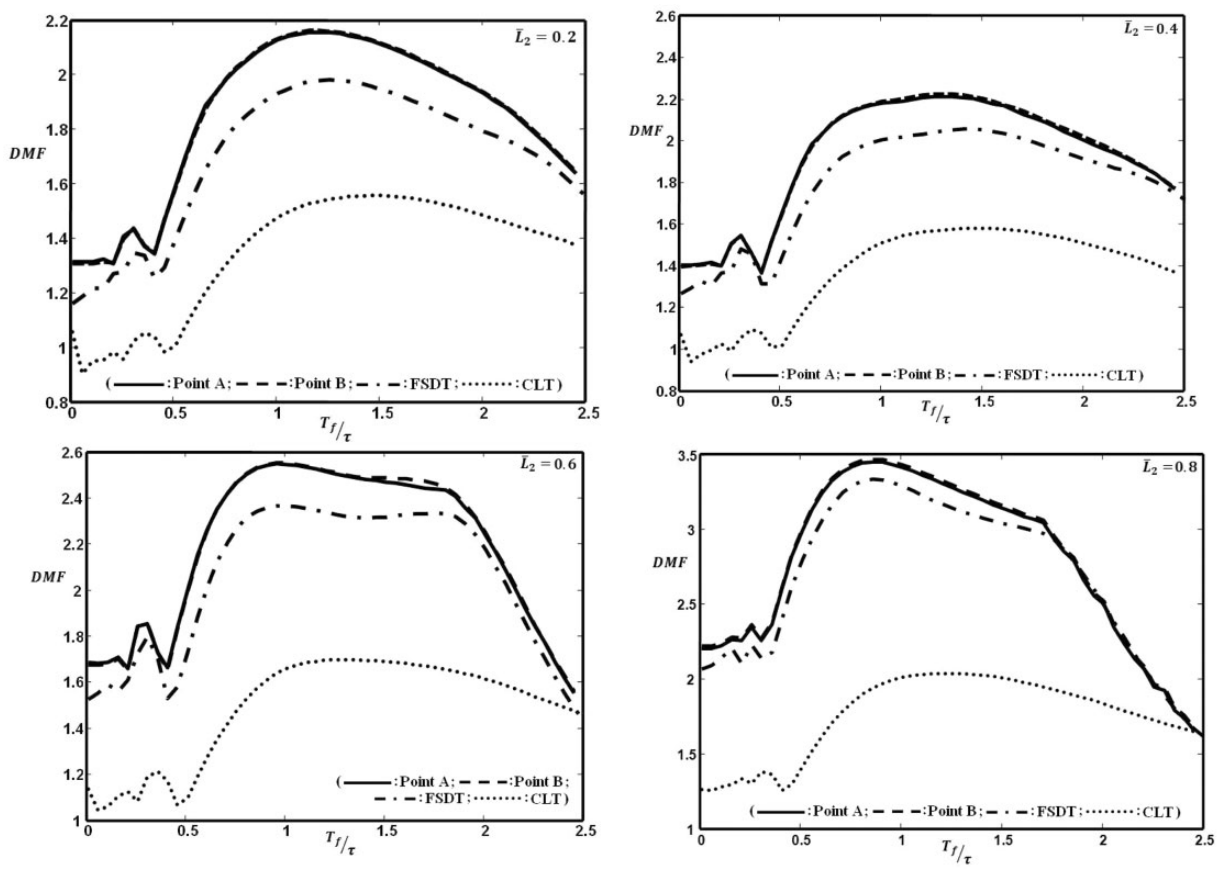

Figure 12. Variation of DMF vs. T_f/τ for different delamination lengths (delamination located at interface 3). DMF: dynamic magnification factor. CLT: classical lamination theory.
CLT: classical lamination theory; FSDT: first-order shear deformation theory.

value for the maximum dynamic response of the considered beam. This is due to the softening effect of higher order terms in the displacement functions that makes the beam more flexible. In addition, the influence of two other parameters i.e. delamination length and its location on different interfaces have fluctuating variations which for brevity their outcomes are listed in Tables 11–13. For example in Table 10, for normalized

Downloaded from jcm.sagepub.com at PENNSYLVANIA STATE UNIV on October 7, 2016

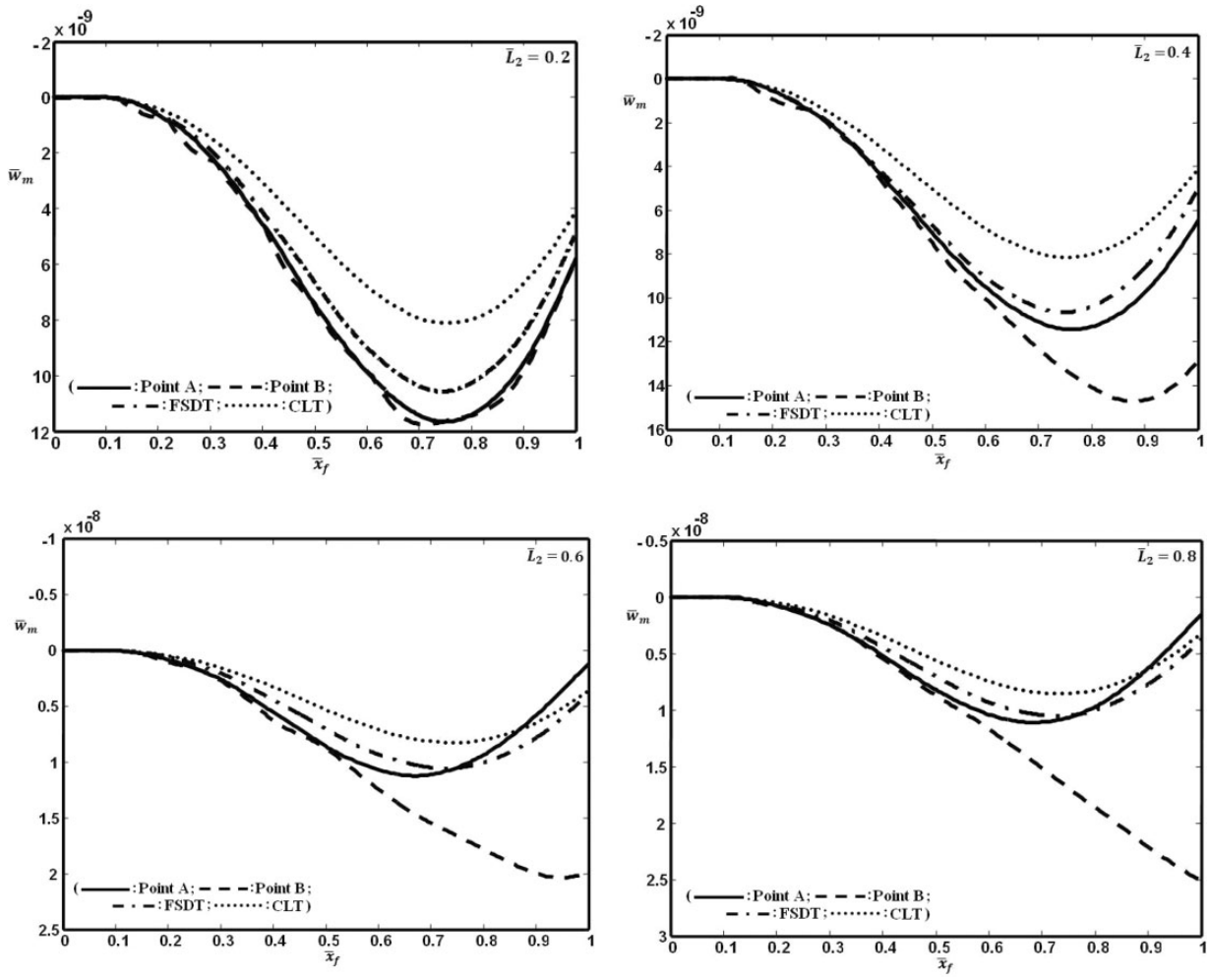

Figure 13. Variation of $\bar{w}_m$ vs. $\bar{x}_f$ for different delamination lengths (delamination located at interface 1). CLT: classical lamination theory.
CLT: classical lamination theory; FSDT: first-order shear deformation theory.

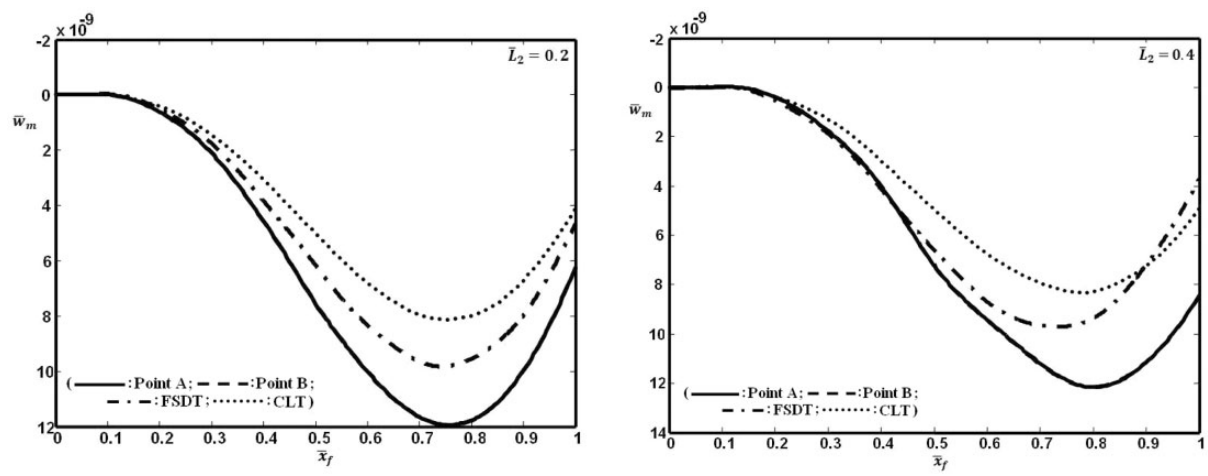

Figure 14. Variation of $\bar{w}_m$ vs. $\bar{x}_f$ for different delamination lengths (delamination located at interface 2). CLT: classical lamination theory.
CLT: classical lamination theory; FSDT: first-order shear deformation theory.

Downloaded from jcm.sagepub.com at PENNSYLVANIA STATE UNIV on October 7, 2016

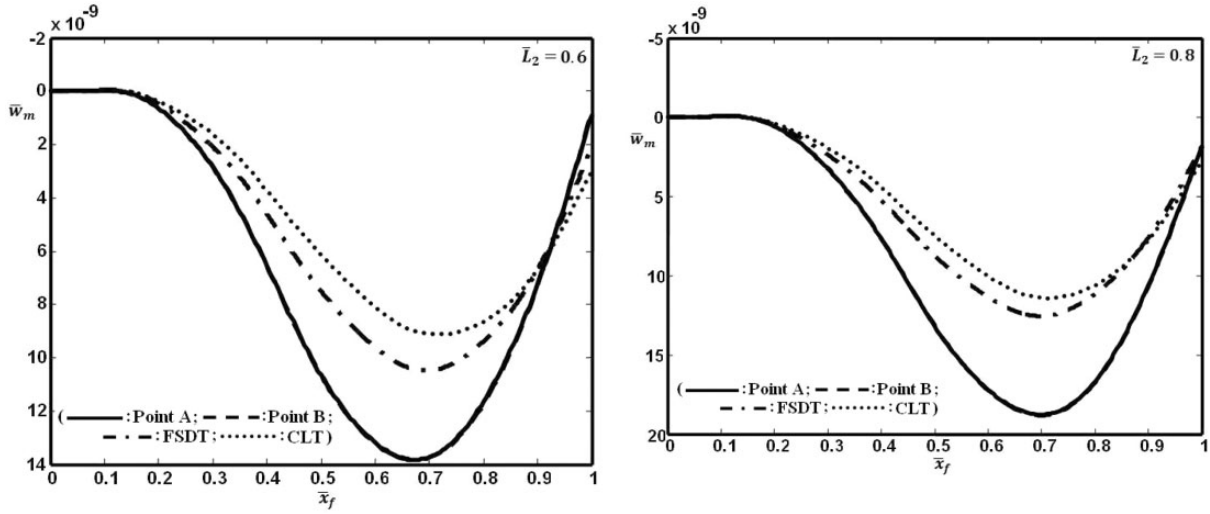

Figure 14. Continued.

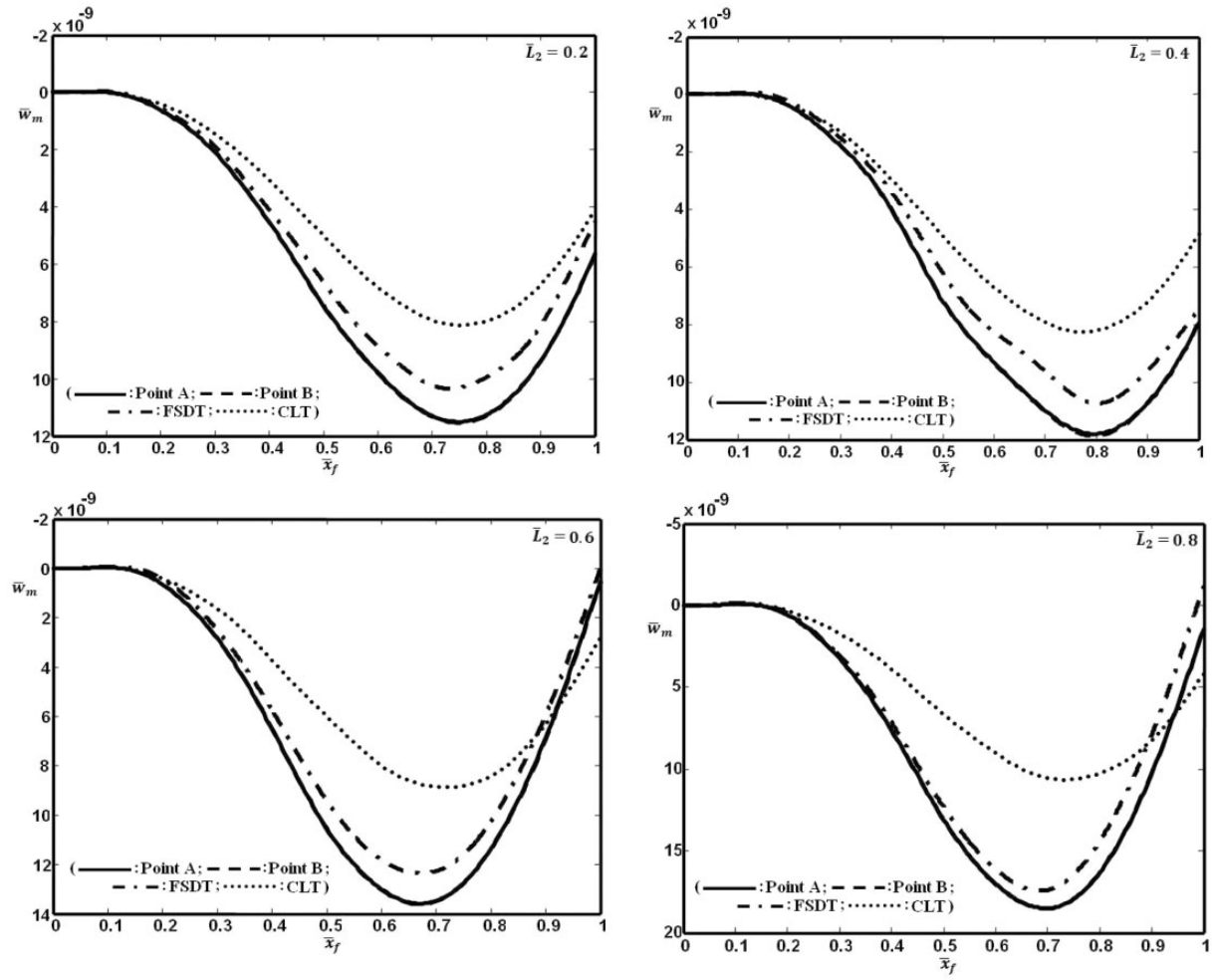

Figure 15. Variation of $\overline{w}_m$ vs. $\overline{x}_f$ for different delamination lengths (delamination located at interface 3). CLT: classical lamination theory.
CLT: classical lamination theory; FSDT: first-order shear deformation theory.

Downloaded from jcm.sagepub.com at PENNSYLVANIA STATE UNIV on October 7, 2016

Table 11. Critical velocity of the force and its position travelling on the laminated composite beam (LCB) with delamination located at interface 1.

	$\bar{L}_2 = 0.2$			$\bar{L}_2 = 0.4$			$\bar{L}_2 = 0.6$			$\bar{L}_2 = 0.8$		
	T_f/τ	v_{cr}	$\bar{x}_f\|_{cr}$	T_f/τ	v_{cr}	$\bar{x}_f\|_{cr}$	T_f/τ	v_{cr}	$\bar{x}_f\|_{cr}$	T_f/τ	v_{cr}	$\bar{x}_f\|_{cr}$
A	1.31	266.4540	0.75	1.26	256.2840	0.76	1.06	215.6040	0.67	1.01	215.6040	0.69
B	1.31	266.4540	0.71	1.21	246.1140	0.88	1.16	235.9440	0.95	1.16	235.9440	1
CLT	1.51	307.1340	0.75	1.46	296.9640	0.75	1.41	286.7940	0.75	1.36	276.6240	0.74
FSDT	1.31	266.4540	0.74	1.26	256.2840	0.75	1.21	246.1140	0.73	1.21	246.1140	0.73

CLT: classical lamination theory; FSDT: first-order shear deformation theory.

Table 12. Critical velocity of the force and its position travelling on the laminated composite beam (LCB) with delamination located at interface 2.

	$\bar{L}_2 = 0.2$			$\bar{L}_2 = 0.4$			$\bar{L}_2 = 0.6$			$\bar{L}_2 = 0.8$		
	T_f/τ	v_{cr}	$\bar{x}_f\|_{cr}$	T_f/τ	v_{cr}	$\bar{x}_f\|_{cr}$	T_f/τ	v_{cr}	$\bar{x}_f\|_{cr}$	T_f/τ	v_{cr}	$\bar{x}_f\|_{cr}$
A	1.31	266.4540	0.75	1.21	246.1140	0.80	0.96	195.2640	0.67	0.86	174.9240	0.70
B	1.31	266.4540	0.75	1.21	246.1140	0.80	1.01	205.4340	0.67	0.86	174.9240	0.70
CLT	1.46	296.9640	0.75	1.46	296.9640	0.78	1.31	266.4540	0.71	1.16	235.9440	0.71
FSDT	1.26	256.2840	0.74	1.26	256.2840	0.73	1.01	205.4340	0.69	0.86	174.9240	0.70

CLT: classical lamination theory; FSDT: first-order shear deformation theory.

Table 13. Critical velocity of the force and its position travelling on the laminated composite beam (LCB) with delamination located at interface 3.

	$\bar{L}_2 = 0.2$			$\bar{L}_2 = 0.4$			$\bar{L}_2 = 0.6$			$\bar{L}_2 = 0.8$		
	T_f/τ	v_{cr}	$\bar{x}_f\|_{cr}$	T_f/τ	v_{cr}	$\bar{x}_f\|_{cr}$	T_f/τ	v_{cr}	$\bar{x}_f\|_{cr}$	T_f/τ	v_{cr}	$\bar{x}_f\|_{cr}$
A	1.31	266.4540	0.75	1.21	246.1140	0.79	0.96	195.2640	0.67	0.86	174.9240	0.69
B	1.31	266.4540	0.75	1.21	246.1140	0.79	0.96	195.2640	0.67	0.86	174.9240	0.69
CLT	1.51	307.1340	0.75	1.46	296.9640	0.78	1.31	266.4540	0.72	1.26	256.2840	0.74
FSDT	1.41	286.7940	0.73	1.26	256.2840	0.80	1.16	235.9440	0.67	1.06	215.6040	0.68

CLT: classical lamination theory; FSDT: first-order shear deformation theory.

delamination length of $\bar{L}_2 = 0.2$ located at the interface 1, the maximum DMF for points A and B occurs at the same value $T_f/\tau = 1.31$ (also see Figure 10). Moreover, from Figure 13 or Table 11, for normalized delamination length of 0.2, the maximum deflection at the beam center occurs when the moving force passes the position of $\bar{x}_f|_{cr} = 0.75$ and 0.71 for points A and B, respectively. Finally, one can observe that when the delamination is located at the interface 1 with normalized length 0.8 the maximum deflection at point B occurs when the moving force passes the beam length i.e. $\bar{x}_f|_{cr} = 1$. This is due to the occurrence of significant opening in the delaminated segments. Moreover, it should be said that the $\bar{x}_f|_{cr}$ is not affected considerably by change of other parameters. It can be further extracted from these tables that the critical velocity predicted by the present formulation, CLT and FSDT decreases as the delamination length increases. Also, it should be noted that the critical velocities predicted by CLT are greater than the value presented in this paper. However, out of these figure and tables one can say the DMF and critical velocities for points A and B are the same when no significant opening occurs in the delaminated interfaces. Whereas, when the opening is considerable (see Figure 13), these points have the different DMF and critical velocities due to the

Downloaded from jcm.sagepub.com at PENNSYLVANIA STATE UNIV on October 7, 2016

dynamic contact. It should be emphasized that Kargarnovin et al.[18] i.e. FSDT in Figures 10–15 has ignored the bending-extension coupling which causes significant differences in the dynamic response.

Conclusion

The current work presents for the first time the solution to the dynamic behavior of a delaminated composite beam when the dynamic contact is considered in the delaminated segments. The combined effects of transverse shear deformation, rotary inertia, material couplings (flexure–tensile, flexure–twist and tensile–twist couplings) and the Poisson's effect are considered in this analysis so that it can be used to predict more realistically the dynamic response of the delaminated LCB with general lay-ups. Based on the finite element approach, the matrix form of governing equations of motion are derived in which the violation of unilateral contact conditions in the delaminated region is prohibited by imposing contact constraints using the Lagrange multipliers. It has been shown that the numerical results are in good agreement with available experimental and analytical data.

Under a moving/non-moving force a thorough study is carried out to investigate the effects of the lay-ups and delamination parameters namely delamination length and its thicknesswise location on the dynamic response of the delaminated LCB such as dynamic deflection and critical velocity and following conclusions are drawn:

- Ignoring the material couplings lead the designers to some wrong conclusions especially when the LCB is vibrating in one of the longitudinal and torsional modes.
- For an angle-ply LCB with ($\theta = 0^\circ$) or ($\theta = 90^\circ$) lay-ups, the inclusion of Poisson's effect produces no significant changes on the fundamental frequency. However, for a angle-ply LCB with lay-ups except $\theta = 0^\circ$ and 90°, the fundamental frequency with no Poisson's effect deviates significantly from the exact value (i.e. considering Poisson's effect), especially for the layout angle between 30° and 60°.
- The influence of dynamic contact between the upper and lower surfaces of the delaminated zone becomes more significant for a delaminated LCB in which differences in the stiffnesses of the sub-beams around delaminated zone get higher due to the lay-ups or thicknesswise location of the delamination.
- It should be mentioned that the dynamic response of the delaminated LCB excited by a harmonic force is greatly dependent on the frequency of the force. The closer the exciting frequency is to the fundamental natural frequency of the delaminated LCB, the greater the response amplitude would be.
- The effect of dynamic contact between the upper and lower segments of the delaminated section becomes more significant for the longer delamination.
- The CLT predicts least value for the maximum dynamic response whereas the presented formulation in this paper gives the highest value for the maximum dynamic response of the considered beam which is more realistic.
- For most cases considered for the LCB under the action of moving force, the maximum dynamic deflection at the beam center occurs when the force passes approximately 70% of the beam length. However, when the significant opening is taken place in the delamination segments, the lower segments in the delamination region reaches its maximum deflection when the force passes the other beam end.
- The critical velocity predicted by the present formulation, CLT and FSDT decreases as the delamination length increases.
- The critical velocities predicted by CLT are greater than the value presented in this paper.

Funding

This research received no specific grant from any funding agency in the public, commercial, or not-for-profit sectors.

Conflict of Interest

None declared.

References

1. Wang JTS, Liu YY and Gibby JA. Vibration of split beams. *J Sound Vib* 1982; 84: 491–502.
2. Mujumdar PM and Suryanarayan S. Flexural vibrations of beams with delaminations. *J Sound Vib* 1988; 125: 441–461.
3. Tracy JJ and Pardoen GC. Effect of delamination on the natural frequencies of composite laminates. *J Compos Mater* 1989; 23: 1200–1215.
4. Yin WL and Jane KC. Vibration of a delaminated beam-plate relative to buckled states. *J Sound Vib* 1992; 156: 125–140.
5. Chang TP and Liang JY. Vibration of postbuckled delaminated beam-plates. *Int J Solids Struct* 1998; 35: 1199–1217.
6. Lee S, Park T and Voyiadjis GZ. Free vibration analysis of axially compressed laminated composite beam-columns with multiple delaminations. *Compos Part B-Eng* 2002; 33: 605–617.
7. Lee S, Park T and Voyiadjis GZ. Vibration analysis of multi-delaminated beams. *Compos Part B-Eng* 2003; 34: 647–659.

Downloaded from jcm.sagepub.com at PENNSYLVANIA STATE UNIV on October 7, 2016

8. Shu D and Della CN. Free vibration analysis of composite beams with two non-overlapping delaminations. *Int J Mech Sci* 2004; 46: 509–526.
9. Shu D and Della CN. Vibrations of multiple delaminated beams. *Compos Struct* 2004; 64: 467–477.
10. Della CN and Shu D. Vibration of beams with double delaminations. *J Sound Vib* 2005; 282: 919–935.
11. Della CN and Shu D. Vibration of delaminated multilayer beams. *Compos Part B-Eng* 2006; 37: 227–236.
12. Della CN and Shu D. Vibration of beams with two overlapping delaminations in prebuckled states. *Compos Part B-Eng* 2007; 38: 109–118.
13. Kargarnovin MH, Ahmadian MT and Jafari-Talookolaei RA. Analytical solution for the dynamic analysis of a delaminated composite beam traversed by a moving constant force. *J Vib Control* 2013; 19(10): 1524–1537.
14. Jafari-Talookolaei RA, Kargarnovin MH and Ahmadian MT. On the dynamic response of a delaminated composite beam under the motion of an oscillating mass. *J Compos Mater* 2012; 46: 2863–2877.
15. Valoor MT and Chandrashekhara K. A thick composite-beam model for delamination prediction by using neural networks. *Compos Sci Technol* 2000; 60: 1773–1779.
16. Shen MHH and Grady JE. Free vibrations of delaminated beams. *AIAA J* 1992; 30: 1361–1370.
17. Luo H and Hanagud S. Dynamics of delaminated beams. *Int J Solids Struct* 2000; 37: 1501–1519.
18. Kargarnovin MH, Ahmadian MT and Jafari-Talookolaei RA. Dynamics of a delaminated Timoshenko beam subjected to a moving oscillatory mass. *Mech Based Des Struct* 2012; 40: 218–240.
19. Kargarnovin MH, Ahmadian MT, Jafari-Talookolaei RA, et al. Semi-analytical solution for the free vibration analysis of generally laminated composite Timoshenko beams with single delamination. *Compos Part B-Eng* 2013; 45: 587–600.
20. Reddy JN. *Mechanics of laminated composite plates and shells: theory and analysis*, 2nd ed., CRC Press, 2003.
21. Jun L, Xiaobin L and Hongxing H. Free vibration analysis of third-order shear deformable composite beams using dynamic stiffness method. *Arch Appl Mech* 2009; 79: 1083–1098.
22. Zienkiewicz OC. *The finite element method*. London: McGraw-Hill, 1977.
23. Jafari-Talookolaei RA, Kargarnovin MH and Ahmadian MT. Free vibration analysis of cross-ply layered composite beams with finite length on elastic foundation. *Int J Comput Meth* 2008; 5: 21–36.
24. Lin YH and Trethewey MW. Finite element analysis of elastic beams subjected to moving dynamic loads. *J Sound Vib* 1990; 136: 323–342.
25. Okafor A, Chandrashekhara K and Jiang YP. Delamination prediction in composite beams with built-in piezoelectric devices using modal analysis and neural network. *Smart Mater Struct* 1996; 5: 338–347.
26. Zhu JF, Gu Y and Tong L. Formulation of reference surface element and its applications in dynamic analysis of delaminated composite beams. *Compos Struct* 2005; 68: 481–490.
27. Krishnaswamy S, Chandrashekhara K and Wu WZB. Analytical solutions to vibration of generally layered composite beams. *J Sound Vib* 1992; 159: 85–99.
28. Jun L, Hongxing H and Rongying S. Dynamic finite element method for generally laminated composite beams. *Int J Mech Sci* 2008; 50: 466–480.
29. Kadivar MH and Mohebpour SR. Finite element dynamic analysis of unsymmetric composite laminated beams with shear effect and rotary inertia under the action of moving loads. *Finite Elem Anal Des* 1998; 29: 259–273.
30. Chandrashekhara K, Krishnamurthy K and Roy S. Free vibration of composite beams including rotary inertia and shear deformation. *Compos Struct* 1990; 14: 269–279.
31. Chandrashekhara K and Bangera KM. Free vibration of composite beams using a refined shear flexible beam element. *Comput Struct* 1992; 43: 719–727.

Appendix I

Lagrange interpolation functions are as follows:

$$N_1(\eta) = 1 - 3\eta + 2\eta^2, \quad N_2(\eta) = 4\left(\eta - \eta^2\right) \text{ and } N_3(\eta) = 2\eta^2 - \eta \tag{33}$$

and Hermite interpolation functions can be written as:

$$\begin{aligned}
\Lambda_1(\eta) &= 1 - 23\eta^2 + 66\eta^3 - 68\eta^4 + 24\eta^5,\\
\Lambda_2(\eta) &= L_e\left(\eta - 6\eta^2 + 13\eta^3 - 12\eta^4 + 4\eta^5\right),\\
\Lambda_3(\eta) &= 16\eta^2 - 32\eta^3 + 16\eta^4,\\
\Lambda_4(\eta) &= L_e\left(-8\eta^2 + 32\eta^3 - 40\eta^4 + 16\eta^5\right),\\
\Lambda_5(\eta) &= 7\eta^2 - 34\eta^3 + 52\eta^4 - 24\eta^5 \text{ and}\\
\Lambda_6(\eta) &= L_e\left(-\eta^2 + 5\eta^3 - 8\eta^4 + 4\eta^5\right)
\end{aligned} \tag{34}$$

Downloaded from jcm.sagepub.com at PENNSYLVANIA STATE UNIV on October 7, 2016